A NEW APPROACH TO ULTRAHIGH RESOLUTION ENDOSCOPIC MEDICAL IMAGING

By

BONGSOO LEE

A DISSERTATION PRESENTED TO THE GRADUATE SCHOOL
OF THE UNIVERSITY OF FLORIDA IN PARTIAL FULFILLMENT
OF THE REQUIREMENTS FOR THE DEGREE OF
DOCTOR OF PHILOSOPHY

UNIVERSITY OF FLORIDA

1999

To my wife, Seunghyun Cho, and my son, Chungwon Lee.

ACKNOWLEDGMENTS

I would first like to acknowledge my supervisory committee. To Dr. Wesley E. Bolch, my adviser, I would like to give thanks and appreciation for his support during my doctoral work. I would also like to thank Dr. James K. Walker for his valued advice, support, and help throughout my doctoral research in Nanoptics, Inc. In addition, I would like to extend my appreciation to Dr. Won Y. Choi for his support and guidance, which helped in the completion of this research. I would like to extend my gratitude to my other committee members, Dr. Alan M. Jacobs and Dr. Samim Anghaie for all their interest in my work and their helpful suggestion.

I would like to thank Nanoptics Inc. for providing various research facilities and fellowship for 3 years. I would also like to thank all Nanoptics members, - Dr. Jacob Tymiansky, Dr. Yong Li, Mr. Jonathan Couch, and Mr. Stephan A. Tuchman - for their support, advice, and the great times we have had.

I would like to extend my gratitude to the Korean Government for awarding me a Korean Government Overseas Scholarship for my doctoral study in the University of Florida.

Finally, I am extremely grateful to my parents and parents-in-law. Without their love and support, this work would not have been possible. I would also like to give special thanks my wife, Seunghyun Cho, and my son, Chungwon Lee, for all their patience, unending love, and support of me and my work.

TABLE OF CONTENTS

page

ACKNOWLEDGMENTS iii

ABSTRACT vii

CHAPTERS

1 GENERAL INTRODUCTION 1

- 1-1 Fiber-Optic Endoscopes 1
- 1-2 Principles of Fiber Optics 3
  - 1-2-1 Total Internal Reflection 3
  - 1-2-2 Optical Fiber 5
  - 1-2-3 Fiber Bundle 10
- 1-3 Advantages of GRIN Fibers for Ultrahigh Resolution Fiber-Optic Imaging Systems 12
  - 1-3-1 Background to GRIN Fiber 12
  - 1-3-2 Image Brightness 14
  - 1-3-3 Image Resolution 18
  - 1-3-4 Time Resolution 19
- 1-4 Dissertation Organization 21

2 POLYMER-POLYMER MISCIBILITY STUDY FOR PLASTIC GRADED INDEX OPTICAL FIBER. 23

- 2-1 Introduction 23
- 2-2 Theory 27
- 2-3 Experimental and Results 28
  - 2-3-1 Methods 29
  - 2-3-2 Results 30
- 2-4 Summary 32

3 IMAGE ASSESSMENT OF FIBER-OPTIC IMAGING SYSTEM 38

- 3-1 Introduction 38
- 3-2 Modulation Transfer Function (MTF) 39
  - 3-2-1 Point Spread Function 42

3-2-2 Line Spread Function 42
3-3-3 Edge Response Function 43

3-3 Crosstalk 44
3-3-1 Background 44
3-3-2 Characterization of Crosstalk 47
3-4 Leaky Rays 55
3-4-1 Background 55
3-4-2 Characterization of Leaky Rays 56
3-5 Summary 62

4 FABRICATION OF PLASTIC GRADED INDEX IMAGE GUIDES FOR ULTRAHIGH RESOLUTION ENDOSCOPES 64

4-1 Introduction 64
4-2 Preparation of GRIN Preforms 68
4-3 Verification of GRIN Properties 73
4-4 Fabrication of GRIN Image Guides 77
4-4-1 First Drawing, Stacking, and Fusing 78
4-4-2 Second Drawing, Stacking, Fusing, and Final Drawing 80
4-4-3 Special Clean Stacking Process 82
4-5 Summary 84

5 FABRICATION OF ULTRAHIGH RESOLUTION PLASTIC GRADED INDEX IMAGE FACEPLATES 85

5-1 Introduction 85
5-2 Preparation of GRIN Preforms 87
5-3 Fabrication of Plastic GRIN Fused Image Faceplates 90
5-4 Special Absorbent Material 91
5-5 Summary 93

6 OPTICAL CHARACTERIZATION OF ULTRAHIGH RESOLUTION PLASTIC GRADED INDEX IMAGE GUIDES AND IMAGE FACEPLATES 95

6-1 Introduction 95
6-2 Optical Characterization of Ultrahigh Resolution Plastic Graded Index Image Guides 96
6-2-1 Image Brightness 96
6-2-2 Image Resolution 103
6-3 Optical Characterization of Ultrahigh Resolution Plastic Graded Index Fused Image Plates 112
6-3-1 Defects 112
6-3-2 Image Resolution 114
6-4 Summary 118

7 CONCLUSIONS AND SUGGESTIONS FOR FUTURE WORK 120

- 7-1 Conclusions 120
- 7-2 Suggestions for Future Work 122
  - 7-2-1 Large Numerical Aperture GRIN Fiber 122
  - 7-2-2 Picosecond Tissue Imaging 123

REFERENCES 125

BIOGRAPHICAL SKETCH 131

Abstract of Dissertation Presented to the Graduate School
of the University of Florida in Partial Fulfillment of the
Requirements for the Degree of Doctor of Philosophy

A NEW APPROACH TO ULTRAHIGH RESOLUTION ENDOSCOPIC MEDICAL IMAGING

By

Bongsoo Lee

August 1999

Chairperson: Wesley E. Bolch
Major Department: Nuclear and Radiological Engineering

Existing fiber-optic imaging systems such as the medical endoscope, boroscope, fused image faceplate, image conduit, and image converter are made from glass step index (SI) fibers. These fiber-optic imaging systems have limitations in both image quality and mechanical properties. In particular, the image resolution of the SI image guide is limited to 5 μm, and the image brightness rapidly diminishes as the microfiber diameter decreases below 5 μm. Thus, it is impossible to develop bright ultrahigh resolution (below 5 μm) fiber-optic image guides with conventional SI fibers.

In this study, ultrahigh resolution image guides and fused fiber-optic faceplates with pixel size between 5 μm and 2.5 μm were fabricated with plastic graded index

(GRIN) fibers. The image brightness and image resolution were measured and compared with those of existing glass SI image guides.

The image brightness of plastic GRIN image guides was more than a factor of two higher than that of glass SI image guides with the same numerical aperture and the same microfiber diameter. There is an improvement in resolution of the plastic GRIN image guides as the microfiber diameter is reduced from 5 μm to 2.5 μm. The modulation transfer function (MTF) of the GRIN image faceplates also improved as the diameter of microfibers decreases below 5 μm.

Through this feasibility study, it has been shown that fiber-optic image guides made from polymeric graded index fibers can achieve ultrahigh image resolution, i.e., below 5 μm with better image brightness than that of SI image guides. The fundamental limitation on the resolution of all previous fiber-optic image guides imposed by the thickness of step index cladding materials can be overcome. This new design of optical systems could have a major impact on a wide array of future optical systems used in defense, industrial, and medical applications.

CHAPTER 1
GENERAL INTRODUCTION

1-1 Fiber-Optic Endoscopes

The name endoscope is derived from two Greek words which are endom (within) and skopein (view) (Haubrich 1989). Endoscope is thus an optical instrument used for viewing internal organs through natural openings (ear, throat, rectum, etc.) or through a small incision in the skin. Generally, a flexible endoscope is referred to as a fiberscope. In flexible endoscopes a bundle of precisely aligned flexible optical fibers is used, while in rigid endoscopes the image is conveyed by a relay of lenses. The classical rigid endoscopes have a number of periscopic and field lens in order to convey the image from distal end to the eyepiece. In some case, as many as 40-50 lenses may cause considerable optical aberration, light losses and ghost images. In addition, the off-centering of lenses can also cause significant vignetting and image deterioration unless great care is taken in the system design. The demands on the performance of endoscopic instruments, which include having a very small diameter and being flexible, have also been increased over the last thirty years. Fiber-optic endoscopes permit the visualization of inaccessible regions in the body without pain and discomfort to the patient. A flexible endoscope is essential for many cases because rigid endoscopes only have a limited use in digestive endoscopy (Salmon 1974). Nearly all current endoscopes often include two kinds of optical fibers for image guide and light guide, and ancillary channels for passage of air, water, and implements such as biopsy forceps, cytology brushes, or various tools which can be remotely controlled (Katzir 1987).

Although the original concept of endoscopy started from the early 19th century, the first endoscope made of optical fibers (fiberscope) was used for viewing the stomach and esophagus in the University of Michigan School of Medicine in 1957 (Hirschowitz 1979). After that time, there has been rapid progress in the development of endoscopes.

Endoscopes can be divided into two categories according to their medical applications (Katzir 1989), although the principles of operation and basic features of the various kinds of fiber-optic endoscopes are similar. The first one includes regular endoscopes such as the gastroscope, colonoscope, and bronchoscope. Gastroscopes are endoscopes for viewing the upper part of the gastrointestinal tract, stomach, esophagus and bile channels. Colonoscopes and bronchoscopes are used for examining the colon and bronchi, respectively. The second category includes ultrathin endoscopes such as needlescopes, ophthalmic endoscopes and angioscopes. In the 1980's, ultrathin fibers were fabricated and the diameter of an endoscope was reduced to less than 1 mm. These kinds of ultrathin endoscopes are used to examine very small parts of internal organs. In recent years, ultrathin silica-based needlescopes have been developed for medical applications such as imaging and clinical diagnostics. The ultrathin needlescopes have 2000 to 6000 pixels and the diameter of them are about 0.2 mm to 0.5 mm. It has been found that it is easy to insert the ultrathin needlescopes to the mammary glands and to detect breast cancer at an early stage (Tsumanuma et al. 1991). In addition, this kind of needlescope makes it possible to obtain real-time images of inaccessible locations within the human body (Kiat et al. 1992). Also, the ophthalmic endoscopes allow a direct viewing of certain internal structures of the eye such as the back side of the iris and the posterior chamber (Rol et al.1995). In general, the ultrathin fiberscopes used in cardiology are called angioscopes which can convey images of the heart valves as well as obstructions (plaques) in the coronary arteries.

Besides transmission of light and images, optical fibers can be used for medical applications in surgery (Artjushenko ey al. 1989), fluorescence methods of diagnosis (Andersson et al. 1987) and high intensity illumination by guiding laser light (Bown 1986). Optical fibers have also been applied to the development of transducers (Lindstrom 1970) or bio-sensors for the measurement and monitoring of many significant parameters in the human body such as temperature, blood pressure, flow of blood and saturation level of oxygen (Tanaka and Benedek 1975, Woldarczyk 1989).

1-2 Principles of Fiber Optics

1-2-1 Total Internal Reflection

Total internal reflection (TIR) is the most important phenomenon for the guiding of light in optical fibers. Under the condition of total internal reflection, light can be completely reflected at a dielectric interface without any reflective coatings. It is required for TIR that the ray of light must be incident on a dielectric interface from the high refractive index to the low refractive side. Figure 1-1 shows that TIR occurs over a certain range of incidence angles. If a ray of light propagates at a certain angle θ_1 ($\theta_1 < \theta_c$) from a high refractive index medium (n_1) to a low refractive index medium (n_2), a portion of light will be reflected back to medium 1 and another part of light will be refracted into medium 2 as shown in Figure 1-1-(a). This behavior of light can be expressed by Snell's law :

$$n_1 \sin\theta_1 = n_2 \sin\theta_2 \tag{1-1}$$

If angle θ_1 is increased to θ_c, θ_2 reaches 90°. The critical angle, θ_c, is defined as,

$$\theta_c = \sin^{-1}\left(\frac{n_2}{n_1}\right) \tag{1-2}$$

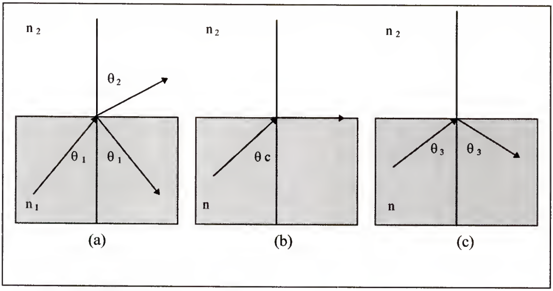

Figure 1-1 Refraction and reflection at the interface between two media with different indices of refraction ($n_1 > n_2$) (a) incident angle $\theta_1 < \theta_c$ (b) incident angle = θ_c (critical angle) (c) incident angle = $\theta_3 > \theta_c$ (Total internal reflection)

At the critical angle θ_c, the refracted ray will travel along the boundary surface (Figure 1-1-(b)). If the angle of incidence is increased further to θ_3 ($\theta_3 > \theta_c$), at the boundary surface the ray is totally reflected back into the higher refractive index medium 1. This phenomenon, shown in Fig. 1-1-(c), is called total internal reflection.

However, when total internal reflection occurs, there must be some electromagnetic field disturbance in the second medium because the phase difference between the incident and totally internally reflected wave is not equal to π. An evanescent wave can exist as light leakage due to the phenomenon of frustrated total internal reflection between two closely spaced or contacted media. In a fiber-optic image bundle, this phenomenon can be significant between adjacent fibers even when the diameter of a fiber is many times greater than the wavelength of light and this evanescent wave coupling between fibers causes light leakage between adjacent fibers over a region where the separation between the fibers is up to a few wavelengths of light (Kapany 1968).

1-2-2 Optical Fiber

An optical fiber is a dielectric wave guide. Light can be transmitted through optical fibers by total internal reflection. Usually optical fibers are flexible, thin, cylindrical and made of transparent materials such as glass or plastic. The most abundant and inexpensive material to make optical fibers is glass and most often this is an oxide glass based on silica (SiO_2) and some additives. Although silica glass is one of the most transparent and low loss materials in the visible wavelength range, in some sensors or medical applications, the fiber length is so short (less than a few meters) that fiber loss and fiber dispersion are not of concern (Yeh 1990). The required properties are optical quality, mechanical strength and flexibility. For these reasons, plastic optical fibers can be used in medical applications, especially in medical endoscopes. Most plastic fibers are made with polymethylmeth-acrylate (PMMA) polymer and its copolymers. There are many advantages to the use of plastic fibers. The processing of plastic fibers is much simpler and less demanding than that for all glass fibers and plastic fibers are lighter and lower cost compared to glass fibers. It is well known that plastic fibers are much more flexible than glass fibers. Using the technique of molecular alignment, a 0.27 mm diameter PMMA based image guide has exhibited unlimited 180^0 flexing cycles with a bending radius of 1.5 mm (Struik 1990). This is to be compared with an 8 mm bending of same diameter glass fiber. On the other hand, it might be a problem for plastic fibers if it has to withstand a high temperature environment. However, PMMA plastic fibers generally can operate within a continuous maximum temperature of 167 ^{o}F (75 ^{o}C). For short duration, it may be subjected up to 212 ^{o}F (100 ^{o}C) maximum.

In general, optical fibers have a cylindrical core and are surrounded by a cladding. The refractive index of the core (n_1) is always higher than that of the cladding (n_2) to guide the light wave. If both n_1 and n_2 are uniform across the cross sections, the fiber is called as a step index fiber (SI) and if n_1 varies with the core radius (i.e., n_1 gradually decreases from the center of the core to the outer radius), it is a gradient or graded index fiber (GRIN). Also optical fibers can be classified as single mode fiber (SMF) and multi-mode fiber (MMF) according to the core size (Hecht 1987).

Consider now in Figure 1-2 a ray incident on the face of the SI fiber at angle A_0. The light will be refracted and will travel through the core by total internal reflection. On the other hand, at the incident angle A_1, a ray will be refracted inside the core and refracted into the cladding. At angle A_c, a ray will be refracted along the boundary of the core and cladding. The angle A_c is referred to as the maximum acceptance angle and θ_c is the critical angle for internal reflection. The angles A_c and θ_c are determined by the refractive indices of core and cladding. Therefore, a ray incident on the core-cladding boundary at an angle less than θ_c will not undergo total internal reflection and finally will be lost. However, at an angle greater than θ_c, a ray will propagate inside the core by a series of internal reflections.

At this point, the relationship between angle and refractive index can be derived based on Snell's law. At the point P_1 in Figure 1-2,

$$n_0 \sin A_c = n_1 \sin(90 - \theta_c) \tag{1-3}$$

Also, at the point P_2

$$n_1 \sin\theta_c = n_2 \sin(90) = n_2 \tag{1-4}$$

From the equation (1-3) and (1-4)

$$n_0 \sin A_c = n_1 \cos\theta_c = (n_1^2 - n_2^2)^{1/2} = NA \tag{1-5}$$

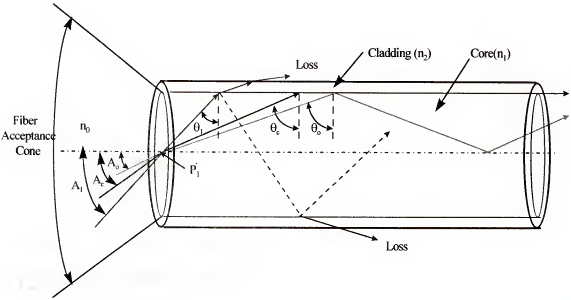

Figure 1-2 Paths of light rays in a step index fiber

NA is the numerical aperture of the SI fiber and defined as the light-gathering power of an optical fiber. When the face of the fiber is in contact with air ($n_o = 1$ for air), NA equals sin θ_c.

Light guiding in a graded index fiber, is shown in Figure 1-3, which can be compared with the picture of light guiding in a step index fiber in Figure 1-2. In SI fiber, the light rays zig-zag between the core/cladding boundary on each side of the fiber axis. In GRIN fiber, the gradient in the refractive index gradually bends the rays back toward the axis.

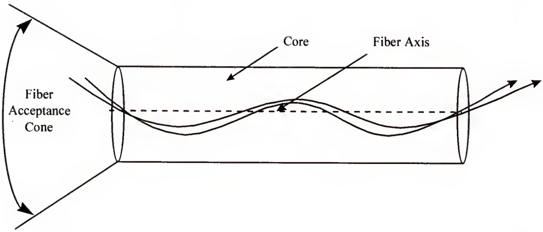

Figure 1-3 Paths of light rays in a GRIN fiber

Suppose the core has the maximum index of n_1 at the center, and the outer edge has index n_2. The index changes gradually from the center of the fiber to a distance *a* from the center, which is the edge of the core. The refractive index profile in GRIN fiber can be expressed as,

$$n(r) = n_2 + C\left[1 - \left(\frac{r}{a}\right)^g\right] \qquad (1\text{-}6)$$

where *C* is a constant of proportionality and *r* is the distance from the fiber axis. The key parameter is *g* which controls the shape of the propagating light rays. For example, if the refractive index falls linearly with radius, *g* would be 1, if it is a parabola, it would be 2. When *g* is infinity, the paths of light rays would be the same as that of SI fiber (Hecht 1987). Figure 1-4 shows the profile of refractive index from core center to the outside edge of the GRIN fiber with different g-values. In communication fibers, the g-value is very important because the bandwidth of the optical fiber depends on this value. When the profile of refractive index in a GRIN fiber is parabolic (g = 2), the bandwidth is maximized.

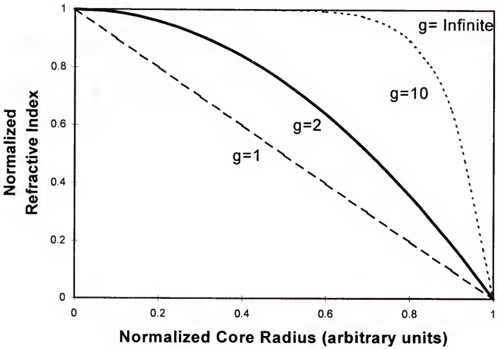

Figure 1-4 The refractive index profile of GRIN fiber with different g-values

1-2-3 Fiber Bundle

It is impossible for a single fiber to transmit an image. An individual fiber can transmit only a spot of light of a certain color and intensity. To transmit an image, a large number of single fibers should be aligned and fused together. This means assembly of optical fibers in which the fibers are ordered in exactly the same way at both ends of the bundle to create an image. This type of fiber bundle is called a coherent bundle or image guide bundle. On the other hand, the assembly of optical fibers that are bundled but not ordered is called an incoherent bundle. This kind of optical fiber bundle which is incapable of producing an image is also used in medical endoscopes, boroscopes and fiberscopes as a light guide. The light guide as well as image guide is essential to construct an image by any optical instruments. They are much less expensive and easy to produce, and are designed to maximize light carrying ability rather than high image resolution. Generally, the individual fibers of a light guide are much thicker (about 30 μm) than fibers in an image guide because resolution is not a factor (Kawahara and Ichikawa 1987).

In an image guide, each fiber core in the bundle captures a portion of the image and delivers it to the other end of the bundle. In this case, the amount of image detail (resolving power) depends on the diameter of each fiber core. If the single fiber core of the input side is half black and half white, the output will be gray. Thus, the fiber core should be small enough to discern black and white and to see much detail. Figure 1-5 shows alignment of fibers and images on the distal and proximal face of a coherent fiber bundle. Figure 1-5-(a) shows a low resolution image guide and its transmitted image on the proximal face, while Figure 1-5-(b) shows a high resolution image bundle and its image. Since, the image guide in Figure 1-5-(b) has double the better resolution, the triangular image is better seen on the proximal face of the fiber bundle.

For a fiber bundle, the resolution can be defined by about half a line pair per fiber core (Yeh 1990). For example, if the individual fiber diameter is 50 μm, cores could resolve 10 line pairs per millimeter (10 lp/mm). Generally, the smaller the fiber core diameter, the greater the image resolution in a unit area of image fiber bundle. However, there are some phenomena which lead to reduced resolution much as crosstalk between individual fibers, and leaky rays from each fiber. These phenomena may deteriorate image quality and can be the main reason for reduction in spatial resolution. These phenomena become more important as the core diameter is decreased. Therefore, the optimum core diameter for a given desired resolution depends on parameters such as cladding thickness, refractive index of the core and the cladding and the wavelength of the incident ray.

The ratio of total core area divided by total fiber surface area is referred to as the packing fraction. The packing fraction is related to the light collection efficiency because all light entering the cladding is lost. The packing fraction is one of the most important parameters in a SI image bundle because the packing fraction is related to the cladding thickness and core diameter. In practice the minimum fixed cladding thickness cannot be less than 1 μm which is about two wavelengths of visible light (Kapany 1960). This limitation is due to the difficulty in production as well as physical optical principles (Kawahara and Ichikawa 1987).

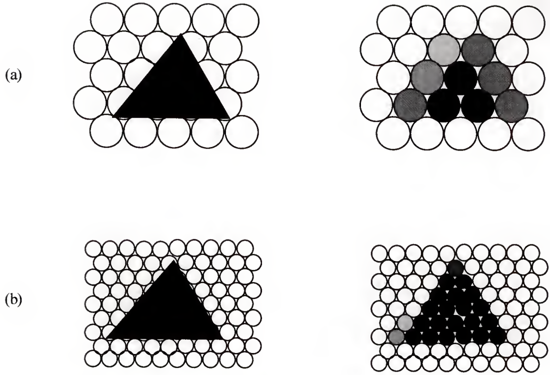

Image projected on the distal face of the fiber bundle

Image seen on the proximal face of the fiber bundle

Figure 1-5 Alignment of optical fibers and images on the distal and proximal face of the image guides. Figure (b) shows 2 times higher resolution image than that of Figure (a)

1-3 Advantages of GRIN Fibers for Ultrahigh Resolution Fiber-Optic Imaging Systems

1-3-1 Background to GRIN Fiber

Plastic optical fibers have been made for about 40 years. It has always been fabricated with a step index (SI) of refraction and has been used in short distance (less than 100 m) fiber-optic communications. A cross section of such a fiber is shown in Figure 1-6. It can be seen that the SI fiber is constructed with a core and cladding with refractive indices n_1 and n_2 respectively, where $n_1 > n_2$.

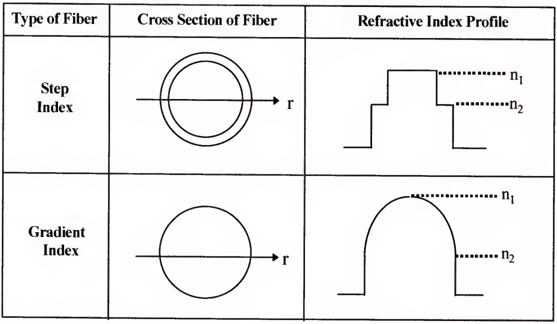

Figure 1-6 The structures of the two basic types of optical fiber

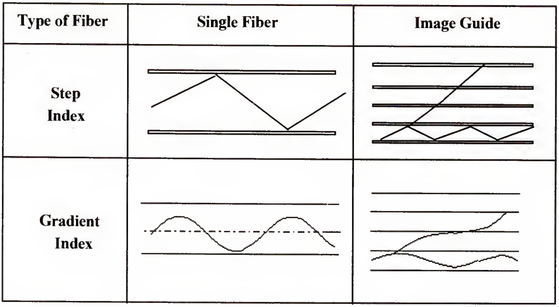

Figure 1-7 The trajectories of typical light rays in SI and GRIN fiber

Glass optical fibers are used in all endoscopes and are made with this SI structure The SI structure can be compared with the GRIN structure which is also shown in Figure 1-6. There are different trajectories of light rays in the two types of fiber. This is shown schematically in Figure 1-7.

In SI fibers, the light travels in straight lines. At angles greater than the critical angle of internal reflection, the light is reflected at the core cladding interface. At angles less than the critical angle, the light is refracted into the cladding, from which it emerges into the adjacent fiber in the SI image guide. This small angle light traverses the various fibers in the image guide until it reaches the side of the image guide and is absorbed.

In GRIN fiber, the light travels in a curved trajectory, always being refracted back towards the axis of the fiber. At angles greater than the critical angle, light never reaches the outer edge of the fiber. At angles less than the critical angle, the light enters the adjacent fiber, traverses the guide, and is absorbed on the periphery of the guide as in the case of the SI guide.

1-3-2 Image Brightness

The brightness, B, of the image transmitted by a guide is defined as (Wang et al. 1995) :

$$B = PF\,(NA)^2\,10^{-\left(\frac{\alpha L}{10}\right)} \qquad (1\text{-}7)$$

where PF (Packing Fraction) is the ratio of the area of the core of SI fibers, (or the area of GRIN fibers) to the total area of the image guide as defined in section 1-1-3. As stated in section 1-2-2, NA_{SI} is the numerical apertures of the SI fiber and is defined as :

$$NA_{SI} = \sqrt{\left(n_{co}^2 - n_{cl}^2\right)} \tag{1-8}$$

The numerical aperture of the GRIN fiber, NA_{GI} is defined differently from NA_{SI} because GRIN fiber has refractive index profile from core to outer edge. The numerical aperture on the axis is given by $NA(0) = (n_{co} - n_{cl})^{1/2}$ which is the same as NA_{SI} away from the axis,

$$NA(r/a) = NA(0)\sqrt{\left(1 - \left(\frac{r}{a}\right)^2\right)} \tag{1-9}$$

It becomes zero for r=0 and the effective numerical aperture of the input cross-section is

$$NA_{GI} = \frac{1}{\sqrt{2}} NA(0) = \frac{1}{\sqrt{2}}\sqrt{\left(n_{co}^2 - n_{cl}^2\right)} \tag{1-10}$$

The quantity of light can be accepted by a GRIN fiber is half of that which can be accepted by a SI fiber and all other things being equal.

The light attenuation coefficient α, is given in units of dB/m, and L is the length of the image guide in units of meters. The approximate values of these parameters for both SI and GRIN image guides are given in Table 1-1.

Table 1-1 Values of parameters describing optimized glass SI image guide, and the expected plastic GRIN image guide

Image Guide	Packing Fraction	NA	α (dB/m)
SI (glass)	Table 1-2	0.43	1.0
GRIN (plastic)	1.0	0.32	1.0

Because the GRIN fiber has no cladding, 100% of the GRIN image guide surface area is available to transmit light compared to 36% for the optimized SI glass image guide whose microfiber diameter is 5 μm. The packing fraction of SI fiber depends on fiber outer diameter and cladding thickness. For 5 μm diameter fibers it has been shown that the optimized ratio of core diameter to cladding thickness for best spatial resolution is 3 (Tsumanuma et al. 1988). However, the thickness of cladding should always be at least 1 μm for any diameter fiber to obtain the resolution of a given fiber diameter (Kawahara and Ichikawa 1987, Tsumanuma et al. 1989). The various packing fractions of SI fiber for different fiber diameters are listed in Table 1-2.

Table 1-2 The packing fractions of SI image guides with different microfiber diameter

Microfiber Diameter	Reduced Resolution Core Dia./Cladding Thickness = 3		Optimum Resolution Cladding Thickness = 1 μm	
	Core Diameter	PF	Core Diameter	PF
5 μm	3	0.36	3	0.36
4 μm	2.4	0.36	2	0.25
3 μm	1.8	0.36	1	0.11
2 μm	1.2	0.36	0	0

The numerical apertures of the two types of guide are comparable. In the case of glass, the high value of NA = 0.43 is achieved by appropriate ionic doping at the expense of deteriorating the transmission to a value of α = 1.0 dB/m (Tsumanuma et al. 1988). For GRIN plastic, a value of NA = 0.32 can be achieved with available polymers. The brightness of the transmitted image has been evaluated using the parameters given in Table 1-1 and Table 1-2. Figure 1-8 shows the relation between brightness and microfiber diameter. We shall assume that the attenuation coefficient α, the length and the outer diameter of both glass SI and plastic GRIN image guide are the same in this comparison.

In this Figure 1-8, the phenomena such as crosstalk and leaky rays which deteriorate image quality are not considered to affect the brightness of GRIN and SI image guides. It is expected that the brightness of image guides is decreased slowly as microfiber diameter is smaller in all three cases because crosstalk between adjacent fibers is more severe in image guides which have smaller microfiber diameter

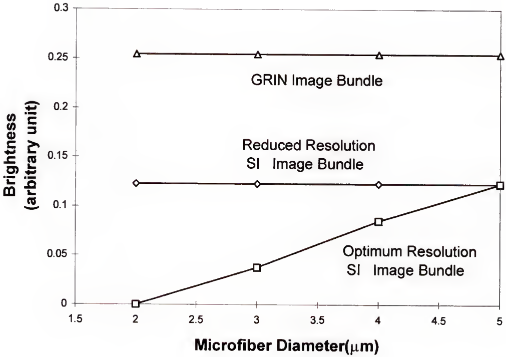

Figure 1-8 Brightness of glass SI image guides and a plastic GRIN guide with different size of microfibers

As shown in Figure 1-8, GRIN image bundle is much brighter than that of an optimum reduced resolution SI image bundle with less than a 5 μm microfiber diameter. In the case of a SI fiber bundle, the core size is reduced to improve resolution, and thus the packing fraction and brightness are also reduced. However, it is possible for GRIN fiber to improve resolution with reducing core size to the physical limit without reducing brightness because there is no need for cladding on GRIN fibers.

1-3-3 Image Resolution

The resolution is improved if a larger number of microfibers is used in the same size image guide. It was reported that there is a limited resolution of the ultrathin SI image guide structure (Tsumanuma et al. 1988). The optimized image guide has a 3 μm core diameter and total fiber diameter of 5 μm microfiber. As stated in section 1-3-2, if the core size decreases below 3 μm in an effort to increase resolution in SI image guide, the image brightness is also decreased.

A guide made of GRIN fiber maintains 100% of light striking the useful area for transmitting light for arbitrary small diameter fiber. The lower limit for the microfiber diameter is about 1 μm, below which no light can be transmitted for fundamental physical reasons. However, there is much potential improvement in resolution from the existing state-of-the-art of 5 μm down to 1.0 μm. If the resolution is improved, the available light per microfiber inevitably decreases. Nevertheless, it is important to have adequate light per microfiber in the image. Existing ultrathin fiberscopes are typically operated at, or near maximum illumination to minimize quantum mottle. It is useful, therefore, to estimate the transmitted light per microfiber (*TL*) as a function of microfiber outer diameter (d). *TL* is calculated by taking the total brightness of the image (*B*) and dividing by the number of fibers in a fixed diameter of, say, 0.25 mm. These predictions and calculations are assuming that the cladding thickness of SI microfibers should be 1 μm to meet the condition of optimum resolution. They are plotted in Figure 1-9 which shows that the GRIN guide has the potential to improve the transmitted light per microfiber (*TL*) for any given resolution below 5 μm diameter.

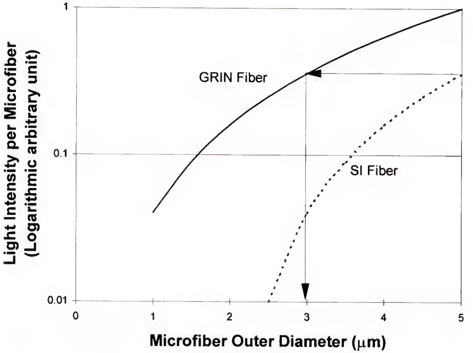

Figure 1-9 Light intensity per microfiber versus microfiber outer diameter

Since the existing ultrathin SI image guide is close to the brightness limit, it can be seen that for the same source illumination level, the microfiber of a GRIN image guide should be able to be reduced down to 3 μm.

1-3-4 Time Resolution

The third major advantage of GRIN image guide lies in its extremely small time dispersion. Historically, the development of GRIN optical fiber was providing a very high bandwidth communication medium. With SI fibers, the distance traveled by the light depends on the angle of its trajectory along the fiber. Since the speed of light is a constant in the SI fiber, there is a variation or dispersion of the arrival times of the light at the end of the fiber. In the case of GRIN fiber, the path length of the light also increases with increasing angle of its trajectory. However, in this case, the speed of the light increases at larger radii due to the decreasing refractive index.

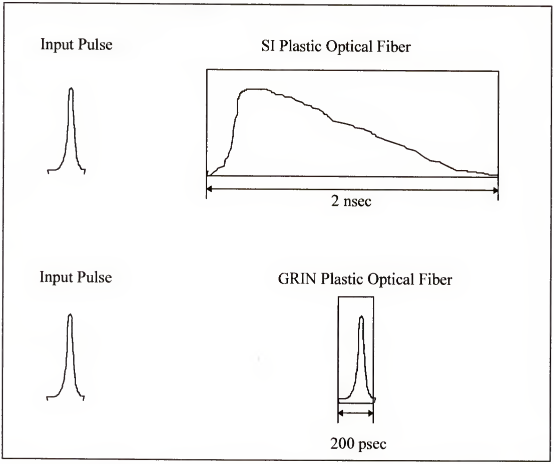

Figure 1-10 Bandwidth measurement by spreading of the output pulse through both SI and GRIN plastic optical fibers with a 20 m length

Figure 1-10 shows the output pulse through a 20 m length SI and GRIN plastic optical fibers (Koike et al. 1991). The output pulse of light from a SI fiber is much more spread than that from GRIN fiber. It is well known that the bandwidth can be maximized when the index profile is optimized in GRIN fiber (Gloge and Marcatili

1973, Halley 1987). The GRIN profile of the fiber can be arranged to minimize the time dispersion to be about 200 times less than that produced by SI fiber. This characteristic of GRIN fiber can be applied to develop a new type of endoscopic in-vivo imaging. It has recently been shown that tissue fluorescence lifetime differences in the range 10 ps to 1 ns can distinguish between specific types of tissue in the body (Dowling et al. 1998). They show that the fluorescence lifetimes of various tissues have at least two exponential components with lifetimes of a few hundred picoseconds and a few nanoseconds. This very short image time dispersion opens the new field of in-vivo biopsy in which cancerous tissues can be visualized.

1-4 Dissertation Organization

The major task of this study is to develop plastic gradient index (GRIN) optical fiber image guides for ultra-high resolution medical endoscopes and image plates. Demonstration of the feasibility of achieving a brighter image with improved resolution and higher flexibility for plastic GRIN endoscopes are the specific goals of this study. Since, the plastic GRIN optical fibers have many advantages compared to step index (SI) optical fiber in fiber optic imaging applications, this study has focused on the verification and demonstration of those advantages of GRIN fibers.

As a general introduction, Chapter 1 provides the necessary fundamentals for understanding the topic. This includes a general background of fiber optic medical endoscopes, principles of fiber optics and advantages of GRIN fibers for the ultrahigh resolution fiber optic imaging systems.

In Chapter 2, a polymer-polymer miscibility study is described. This study assisted in choosing the production process of plastic GRIN image guides and image plates.

Since, most theoretical approaches to fiber optic phenomena are mainly related to optical fibers used in communications, a theoretical discussion of fiber optic imaging is given in Chapter 3.

The fabrication of plastic GRIN image guides for ultrahigh resolution medical endoscopes and image plates are described in Chapters 4 and 5, respectively. The fiber optic image quality such as resolution and brightness are characterized and the discussion of this work is given in Chapter 6. The spatial resolutions are obtained by measuring edge response functions using specially designed optical instruments. In addition, the brightness of GRIN image guides is also obtained by measuring the attenuated power and numerical aperture of optical fibers. All results are compared with known data of glass step index image guides.

Finally, conclusions of all these studies are drawn and future work is suggested in Chapter 7.

CHAPTER 2
POLYMER-POLYMER MISCIBILITY STUDY FOR PLASTIC GRADED INDEX OPTICAL FIBER

2-1 Introduction

The gradient or graded index (GRIN) optical fiber is an inhomogeneous medium in which the refractive index is slowly reduced from the center to the outside of fiber. The GRIN fiber has unique and useful optical characteristics, and it has many applications including optical fiber communication (Ishigure et al. 1996, 1997), use as lens in endoscopes (Leiner and Prescott 1983), compact disc system (Nishi et al. 1986), and various optical instruments (Rees 1982). Both glass and polymer have been used to make GRIN optical fibers. To produce glass GRIN fibers, several methods such as ion exchange (Pearson et al. 1969, Samuels 1990), sol-gel leaching (Shingyouchi and Konishi 1990) and chemical vapor deposition (Pickering et al. 1986) have been used. The glass GRIN fibers have limitations such as poor flexibility, difficulty in processing and a high cost. On the other hand, polymer GRIN fibers have many advantages such as good flexibility, easy to process and lower cost compared to its glass counterparts.

To fabricate polymer GRIN fibers, a few methods such as interfacial-gel polymerization (Ishigure et al. 1994) or copolymerization (Koike et al. 1988, Ohtsuka et al. 1990), photocopolymerization (Koike et al. 1984) and extrusion (Koike 1991, Koike and Nihei 1993, 1995 and 1997) have been suggested. The first three methods are based on the preform rod manufacturing and subsequent fiber drawing technique. These methods utilize a mixture of two monomers or additives with different reactivity or diffusivity.

The extrusion method was recently suggested to produce plastic GRIN fibers using diffusional characteristics of low molecular weight materials (Ho et al. 1995, Koike and Nihei 1997). A new extrusion method for the fabrication of plastic GRIN fiber is recently reported (Park and Lee 1999). It is a continuous process and is capable of controlling the refractive index profile by mechanical means. For several of these methods, the selection of adequately miscible polymers is essential to make good optical quality polymer GRIN fibers.

Nearly all polymer-polymer mixtures were believed to be immiscible or incompatible, but the number of miscible polymer blends has increased due to fundamental research on polymer blends (Olabisi 1979). Prior to 1975, "incompatibility" was used in polymer blending as the rule and "compatibility" as the exception. The term "incompatibility" referred to the formation of more than one phase on mixing and "compatibility" refers to the formation of a single-phase mixture on blending of two polymers. Today, the term "miscibility" is used preferably by some authors to avoid the confusion associated with the less precise technological usage of the term compatibility and for more precise scientific meaning with regard to an equilibrium of mixing or solubility (Paul and Sperling 1986).

It is necessary to define some terminology about polymer-polymer miscibility. Also, Figure 2-1 shows interrelations in polymer blend.

Polymer : Polymeric material or resin with linear, branched or crosslinked structure.

Copolymer : Polymeric material synthesized from more than a single monomer.

Engineering polymer (EP) : A processable polymeric material, capable of being formed to precise and stable dimensions, exhibiting high performance at the continuous use temperature above 100 °C, and having tensile strength in excess of 40 Mpa.

Polymer blend (PB) : A mixture of at least two polymers or copolymers.

Homogeneous polymer blend (HPB) : A mixture of two homogeneous polymers, usually narrow molecular weight distribution fraction of the same polymer.

Miscible polymer blend (MPB) : Polymer blend homogeneous down to the molecular level, associated with the negative of the free energy of mixing.

Partially miscible polymer blend : A sub-class of PB including those blends that exhibit two or more phase at all compositions and temperatures.

Immiscible polymer blend : Any polymer blend whose free energy of mixing is positive.

Compatible polymer blend : A utilitarian term indicating a commercially attractive polymer mixture, normally homogeneous to the eye, frequently with enhanced physical properties over the constituent polymers.

Polymer alloy (PA) : An immiscible polymer blend having a modified interface and/or morphology.

Compatibilization : A process of modification of interfacial properties of an immiscible polymer blend, leading to the creation of a polymer alloy.

Interpenetrating polymer network (IPN) : A sub-class of PB reserved for mixtures of two polymers both components from continuous phase and at least one is synthesized or crosslinked in the presence of the other.

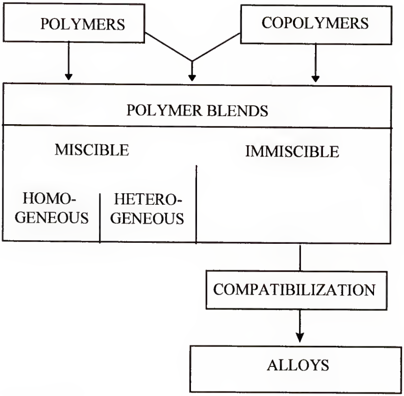

Figure 2-1 Interrelations in polymer blend nomenclature

In this study, a few miscible polymers which are used in copolymerization of GRIN material are selected to examine optical transmittance of their copolymers according to the different polymer fractions by weight. A major thrust in this approach is the idea that long-term GRIN material stability is more easily achieved using a blend of polymers. This approach totally eliminates all concern of the fundamental non-equilibrium state of low molecular weight additives in a polymer matrix. The use of additives to create a refractive index profile can deteriorate the long term mechanical and thermal properties of GRIN fibers. Generally, a GRIN fiber which is made by interfacial-gel polymerization has a tendency to lose GRIN characteristics because the utilized low molecular weight additives can easily diffuse out from the GRIN fiber at high temperature. However, the price to be paid for this new approach is the rather limited number of miscible polymers produced.

2-2 Theory

Generally, a mixture of polymers do not form stable single-phase systems. The negative free energy of mixing is required to achieve miscibility in a mixture of two polymers. The equilibrium state of a polymer mixture is understood in terms of the free energy of mixing (Paul and Newman 1978, Eisel 1990), which can be written as

$$\Delta G_m = \Delta H_m - T\Delta S_m \qquad (2\text{-}1)$$

where ΔG_m is the Gibbs' free-energy change upon mixing, T is the absolute temperature, and ΔH_m , ΔS_m are the enthalpic and entropic contributions, respectively. A negative value of ΔG_m indicates that the solution process will occur spontaneously. The term $T\Delta S_m$ is always positive because there is an increase in the entropy on mixing (Sperling 1992). Therefore the sign of ΔG_m can be decided by ΔH_m, the enthalpy of mixing. For a truly miscible blend, the requirements are

$$\Delta G_m < 0 \qquad (2\text{-}2)$$

$$\left(\partial^2 \Delta G_m / \partial \Delta \phi_i^2\right)_{\mathrm{T,P}} > 0 \qquad (2\text{-}3)$$

where ϕ_i is the volume fraction of the i th component in the blend.

Equation 2-1 can be rewritten on a volume basis for polymer 1 and 2 with volume fraction ϕ_i according to the simplistic Flory-Huggins lattice theory (Utrachi 1989).

$$\frac{\Delta G_m}{VkT} = \frac{g}{V_S}\phi_1\phi_2 + \left[\frac{\phi_1}{V_1}\ln\phi_1 + \frac{\phi_2}{V_2}\ln\phi_2\right] \tag{2-4}$$

The first term on the right-hand side represents the enthalpic contribution per segment volume V_s and the term in brackets demonstrates the entropic contribution to the total free energy of mixing. The entropic effect on enhancing miscibility is small due to the large molecular volumes V_1 and V_2 of macromolecules. Usually, the enthalpic contributions, ΔH_m dominate in the determination of miscibility, especially for non H-bonding blends (Landry et al. 1994). In the majority of cases the enthalpic interaction term is positive, but it can be negative when there is significant interaction between constituent polymers. Hence, a generally accepted method of designing thermodynamic miscibility for a blend is through incorporation of specific attractive groups. This may be done by copolymerizing with monomers containing interaction groups. Two possibilities for these purposes are a copolymer blended with a homopolymer and two copolymers blended. In each case, the two blended polymers could have a common monomer, or monomers with interacting groups.

2-3 Experimental and Results

To achieve high optical transmission, the polymers must be capable of being blended homogeneously down to the molecular level, i.e. miscible, to achieve the desired refractive index profile. As a consequence, the refractive indices of these polymers should be different from each other. Additional constraints on the choice of polymer blends are the followings. First, the material should have as little water absorption as possible, and preferably less than PMMA which can absorb up to 2% of water by weight. Second, the glass transition temperature should be at least 80 °C to ensure mechanical stability. This compares to about 65 °C for the GRIN plastic optical fiber (GI POF) produced by adding additives in acrylic polymer. Third, the bulk light attenuation in the material should be small. Last, the monomer cost should be low.

For polymer-polymer blend experiments, three monomers i.e. methylmethacrylate (MMA), benzylmethacrylate (BMA) and trifluoroethylmethacrylate (3FMA) were used in this study to synthesize copolymers. For GRIN production, it is required to use two polymers P_1 and P_2 with refractive indices n_1 and n_2 respectively. The refractive indices of poly-MMA(PMMA), poly-BMA(PBMA) and poly-3FMA(P3FMA) are 1.49, 1.568 and 1.42 respectively. Figure 2-2 shows the structural formulas of the three monomers.

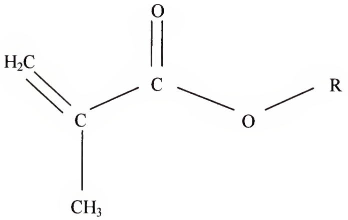

Figure 2-2 Structural formulas of the methylmethacrylate (MMA, $R=CH_3$), benzylmethacrylate (BMA, $R=CH_2C_6H_5$) and trifluoroethyl methacrylate (3FMA, $R=CH_2CF_3$)

2-3-1 Methods

All the monomers were distilled before copolymerization to get rid of any impurities which can cause bubbles during the polymerization process. Bubbles in the polymer are a major factor for decrease in optical transmittance.

Copolymers of MMA / BMA, MMA / 3FMA and BMA / 3FMA in different fractions by weight were synthesized by bulk thermal polymerization. In the case of MMA / BMA system,

P_1 = P(X% BMA + (1-X) % MMA) and P_2 = P((1-X)% BMA + X % MMA)

The copolymers of P_1 and P_2 were cast from solutions of methylene chloride to form films whose transparencies were measured. If the film transparency is 100% than copolymers P_1 and P_2 are totally miscible. Similar studies were carried out for increasing difference in monomer content.

2-3-2 Results

Non-fluorinated system

The copolymers of methylmethacrylate (MMA) and benzylmethacrylate (BMA) in different fractions by weight were synthesized. For example,

P_1 = P(60% BMA + 40% MMA) and P_2 = P(40% BMA + 60% MMA)

We have found that copolymers P_1 and P_2 are miscible over the full range of 0 to 100% of P_1. This result is shown in Figure 2-3. We next studied the polymers,

P_1 = P(70% BMA + 30% MMA) and P_2 = P(30% BMA + 70% MMA)

For the above copolymers, miscibility in the full compositional range of P_1 and P_2 can be achieved (Figure 2-4). At the more extreme differential monomer content,

P_1 = P(80% BMA + 20% MMA) and P_2 = P(20% BMA + 80% MMA)

the range of miscibility is attenuated (Figure 2-5). The refractive index of a given blend of copolymer P_1 and P_2 is determined by the weight fraction and refractive index of each copolymer. The maximum difference in refractive index of the full miscible blends of

P_1 and P_2 was 0.031. If this material composition is used in GRIN plastic optical fibers, it will result in an acceptable numerical aperture, NA = 0.24.

Partially fluorinated system

Two partially fluorinated material systems were examined to measure transparencies of copolymers for increasing difference in monomer content. The case A is

$P_1 = P(X\ \%\ MMA + (1 - X)\ \%\ 3FMA)$, $P_2 = P((1 - X)\ \%\ MMA + X\ \%\ 3FMA)$

and the case B is

$P_1 = P(X\ \%\ BMA + (1 - X)\ \%\ 3FMA)$, $P_2 = P((1 - X)\ \%\ BMA + X\ \%\ 3FMA)$

These systems offer slightly better light transmission than that of non fluorinated systems and very low water absorption. Results of case A are shown in Figure 2-6, 2-7 and 2-8. In Figure 2-6, if X is 35% i.e.,

$P_1 = P(35\ \%\ MMA + 65\ \%\ 3FMA)$ and $P_2 = P(65\ \%\ MMA + 35\ \%\ 3FMA)$

are miscible over the full concentration range. In this case, the maximum refractive index change in 0.021 corresponding to the acceptable numerical aperture of 0.175. This system has some advantages which are very low water absorption, slightly better light transmission than acrylic, the lowest cost of any partially fluorinated monomer and high glass transition temperature (about $90^{o}C$). However, the numerical aperture is rather low owing to the small difference of refractive index between two copolymers.

The material system B appears to be almost completely immiscible as shown in Figure 2-9, 2-10 and 2-11. This material system can not be used to copolymerize GRIN preforms for optical fibers.

2-4 Summary

Several polymer systems have been investigated to test polymer-polymer miscibility for fabrication of plastic GRIN material. Two candidate systems are copolymers of benzyl methacrylate (BMA) and methyl methacrylate (MMA), and copolymers of methyl methacrylate (MMA) and trifluoroethyl-methacrylate (3FMA). These systems offer the advantage of polymeric material with no low molecular weight additives, a controlled numerical aperture up to about 0.25 and low moisture absorption.

These results will be very useful to copolymerize GRIN preforms which are drawn to GRIN fibers. They are also used to fabricate GRIN image guides and fused image face plates. In considering the two candidate systems, the copolymers using MMA and BMA provide better numerical aperture and miscibility over a wider range. Therefore, distilled MMA and BMA monomers were used to produce GRIN preforms by the interfacial-gel copolymerization method.

In further studies, beyond the scope of this thesis, the blends of PMMA and the copolymer (75% Stylene + 25% Acrylonitrite) will be examined. It has been known the two polymers are completely miscible (Adler et al. 1974). In addition, the glass transition temperature is more than 100 °C over the full range of composition of the blend. This system can provide a maximum numerical aperture, NA = 0.32. The fully fluorinated material system also will be studied.

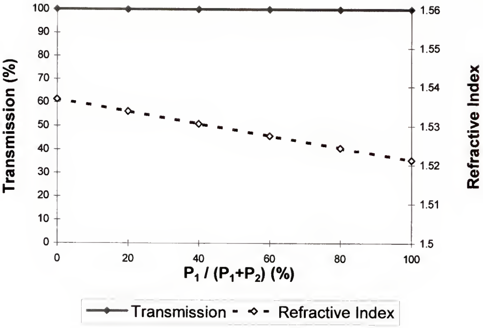

Figure 2-3 Transmission spectra of blends of copolymers P_1 and P_2 together with the resulting refractive indices (Non-fluorinated system). P_1 = 40% BMA / 60% MMA, P_2 = 60% BMA / 40% MMA

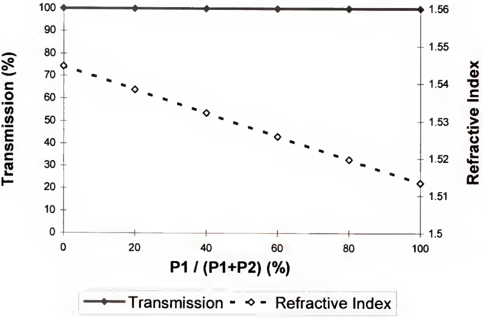

Figure 2-4 Transmission spectra of blends of copolymers P_1 and P_2 together with the resulting refractive indices (Non-fluorinated system). P_1 = 30% BMA / 70% MMA, P_2 = 70% BMA / 30% MMA

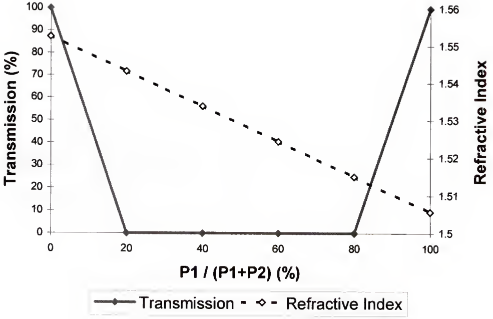

Figure 2-5 Transmission spectra of blends of copolymers P_1 and P_2 together with the resulting refractive indices (Non-fluorinated system). P_1 = 20% BMA / 80% MMA, P_2 = 80% BMA / 20% MMA

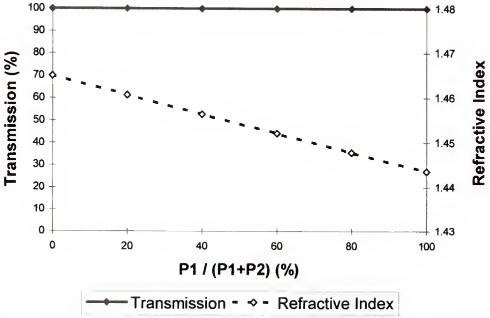

Figure 2-6 Transmission spectra of blends of copolymers P_1 and P_2 together with the resulting refractive indices (Partially-fluorinated system). P_1 = 35% MMA / 65% 3FMA, P_2 = 65% MMA / 35% 3FMA

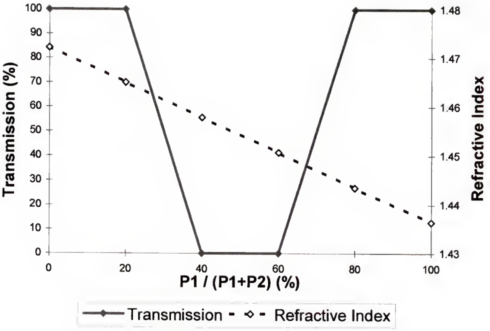

Figure 2-7 Transmission spectra of blends of copolymers P_1 and P_2 together with the resulting refractive indices (Partially-fluorinated system) P_1 = 25% MMA / 75% 3FMA, P_2 = 75% MMA / 25% 3FMA

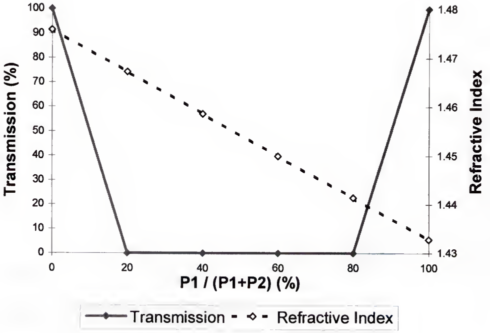

Figure 2-8 Transmission spectra of blends of copolymers P_1 and P_2 together with the resulting refractive indices (Partially-fluorinated system). P_1 = 20% MMA / 80% 3FMA, P_2 = 80% MMA / 20% 3FMA

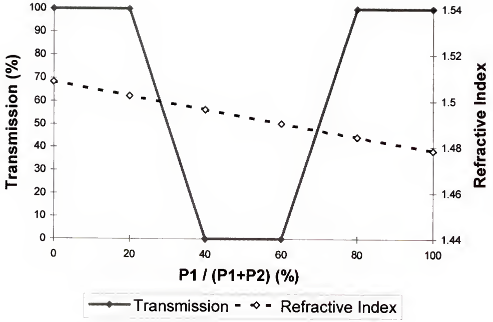

Figure 2-9 Transmission spectra of blends of copolymers P_1 and P_2 together with the resulting refractive indices (Partially fluorinated system). P_1 = 40% BMA / 60% 3FMA, P_2 = 60% BMA / 40% 3FMA

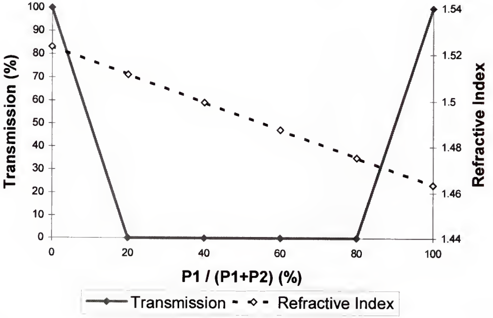

Figure 2-10 Transmission spectra of blends of copolymers P_1 and P_2 together with the resulting refractive indices (Partially fluorinated system). P_1 = 30% BMA / 70% 3FMA, P_2 = 70% BMA / 30% 3FMA

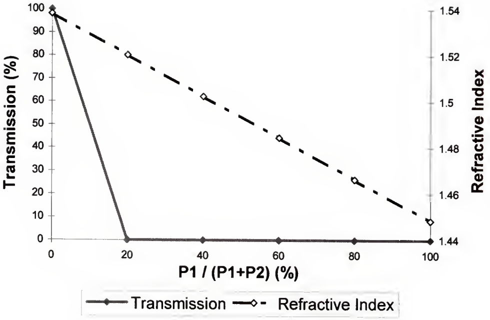

Figure 2-11 Transmission spectra of blends of copolymers P_1 and P_2 together with the resulting refractive indices (Partially fluorinated system). P_1 = 20% BMA / 80% 3FMA, P_2 = 80% BMA / 20% 3FMA

CHAPTER 3
IMAGE ASSESSMENT IN FIBER-OPTIC IMAGING SYSTEM

3-1 Introduction

There are various methods to measure the image forming characteristics of fiber-optic imaging devices. A large number of parameters can affect the image quality in fiber optics (Kapany 1968). These are fiber diameter, spacing between fiber center to center, fiber cross sectional shape, fiber length, fiber numerical aperture, the ratio of the fiber numerical aperture, and the angle of incident light, waveguide coupling between adjacent fibers, light leakage between fibers due to scattering and other imperfections, and change in fiber numerical aperture caused by changing the fiber shape at the ends. These parameters should be considered as important factors in the image transmission quality of fibers. However, it is considered to be very difficult to assess all the parameters in a consistent way.

Two basic image characteristics, spatial resolution and image contrast, are generally used to describe the fiber-optic imaging system, and, they are closely associated with all parameters which were mentioned previously. The spatial resolution is defined as an ability to distinguish or separate two small objects placed close by. In particular, the spatial resolution or the amount of image detail in the fiber-optic imaging system is mainly determined by the diameter of the individual microfibers. The image contrast is the relative difference in image brightness between the object and its background.

For assessing general optical image quality, several methods such as the star pattern test, the square wave or bar test chart, edge response measurement, energy density measurement in the point image have been used (Kapany and Burke 1962). Similarly, for fiber-optic image characterization, the following methods have been used : (1) line resolution, (2) edge response, (3) flux through a hole, and (4) modulation transfer function (Kapany 1968). The modulation transfer function measurement is the most popular image assessment method in fiber optic-imaging systems.

Two complicated phenomena known as crosstalk and leaky rays lower the spatial resolution and the contrast of a transmitted image, thus deteriorating the image quality in a fiber-optic imaging system. They are studied in detail in this chapter.

3-2 Modulation Transfer Function (MTF)

Most imaging systems are often tested by forming an image of a target which has high contrast. The lines of the target are either black on a white background or white on a black background. Realistic objects are rarely black and white but rather they are in shades of gray. Actually, two low-contrast lines fuse more easily into one line than two lines of the same spacing but high contrast. Therefore, any determination of resolution must consider the contrast. Contrast is defined as :

$$C=\frac{E_{\max}-E_{\min}}{E_{\max}+E_{\min}} \tag{3-1}$$

where C is contrast E_{max} and E_{min} are the maximum and minimum amount of light, respectively. Figure 3-1 shows sinusoidal light distribution as function of space. In Figure 3-1, two new parameters can be introduced (Meyer-Arendt 1989).

$$a = (E_{max} - E_{min}) / 2 + E_{min} \tag{3-2}$$

$$b = E_{max} - a \tag{3-3}$$

The ratio of the two parameters is called modulation, M

$$M = \frac{b}{a} \tag{3-4}$$

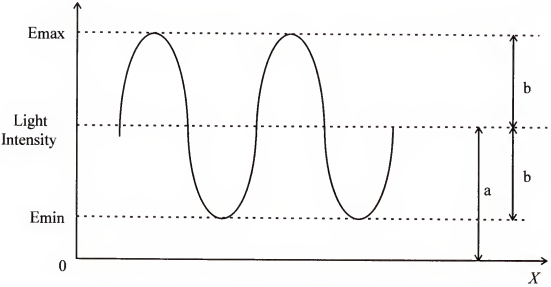

Figure 3-1 Sinusoidal light intensity distribution as function of space in one dimension *X*

With the definition of modulation, modulation transfer factor, *T,* can be defined as the ratio of modulation in the image to modulation in the object.

$$T = \frac{M_{image}}{M_{object}} \tag{3-5}$$

For example, if the image modulation is one-half the object modulation, the modulation transfer factor is 0.5 as shown in Figure 3-2.

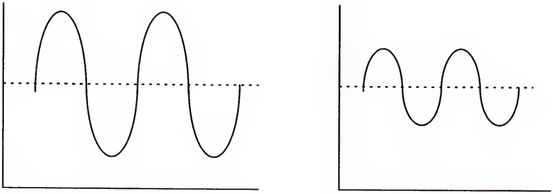

Object

Image

Figure 3-2 The image has half the modulation of the object and the modulation transfer factor is 0.5

The modulation transfer factor T of a given imaging system varies as a function of spatial frequency. The dependence of modulation transfer factor on spatial frequency is related to the number of lines or other detail which can be distinguished from each other, within a given length in the object. Generally, the higher the spatial frequency which is quoted for a system, the better the resolution of a given optical system. Therefore, the modulation transfer factor which is a function of spatial frequency is called modulation transfer function (MTF) which characterizes the blur or spatial resolution of an imaging system at any spatial frequency (Ghatak and Thyagarajan 1978).

3-2-1 Point Spread Function

The spatial resolution of an imaging system can be defined by its point spread function (PSF). The mathematical expression of an infinitesimal point object and its point spread function are as follows.

$$\text{point}\,(x,y) = \delta(x)\,\delta(y) \tag{3-6}$$

$$\text{PSF}\,(x,y) = T\,[\text{point}\,(x,y)] \tag{3-7}$$

Theoretically, the PSF is obtained by transforming (T) the image of an infinitesimal point object, where T is the linear transform of the imaging system. The modulation transfer function, which is the most important and useful descriptor of the spatial resolution of an imaging system, is obtained from the two-dimensional Fourier Transform (F) of the PSF.

$$\text{MTF}\,(u,v) = F\,[\text{PSF}\,(x,y)] \tag{3-8}$$

However, practically it is difficult to determine the point spread function since an infinitesimal point object cannot be produced. Instead, the line spread function (LSF) is introduced to relieve those technical difficulties of measuring the PSF (Hasegawa 1991).

3-2-2 Line Spread Function

The line spread function is a one-dimension representation of the two-dimensional PSF. The LSF can be obtained with a infinitesimal line source, rather than an infinitesimal point aperture in the PSF. The width of the line source should be sufficiently narrow so that its finite extent does not contribute to the width of the image. The mathematical definition of the line source is

$$\text{line}\,(x) = \delta(x) = \int_{-\infty}^{\infty} \delta(x)\,\delta(y)\,dy = \int_{-\infty}^{\infty} \text{point}\,(x,y)\,dy \qquad (3\text{-}9)$$

By using of the line transform T, the line spread function LSF(X) is obtained.

$$\begin{aligned} \text{LSF}\,(x) &= \text{T}\,[\text{line}\,(x)] \\ &= \text{T}\,[\int_{-\infty}^{\infty} \text{point}\,(x,y)\,dy] = \int_{-\infty}^{\infty} \text{PSF}\,(x,y)\,dy \qquad (3\text{-}10) \end{aligned}$$

It is also possible to obtain the MTF from the Fourier Transform of the line spread function (Gaskill 1978, Duffieux 1983).

$$\begin{aligned} \text{F}\,[\text{LSF}\,(x)] &= \int_{-\infty}^{\infty} \text{LSF}\,(x)\exp(-2\pi\,\text{i}ux)dx \\ &= \int_{-\infty}^{\infty}[\int_{-\infty}^{\infty} \text{PSF}\,(x)\exp(-2\pi\, iux)dy\,]\,dx \\ &= \{\int[\int \text{PSF}\,(x)\exp[-2\pi i(ux+vy)]\,dy]\,dx\}_{v=o} \\ &= \text{F}\,[\text{PSF}(x,y)]_{v=0} \\ &= \text{MTF}\,(u,0) \qquad (3\text{-}11) \end{aligned}$$

According to the above mathematical expression, the MTF of the system is evaluated in one dimension by the Fourier Transform of the line spread function.

3-2-3 Edge Response Function

Another method to define the MTF of an imaging system is to use the edge response function. The edge response function (ERF) is obtained with a sharp edge of an object which transmits light only on one side of itself. Hence, its transmission can be mathematically defined by a step function.

$$\begin{aligned} \text{STEP}\,(x,y) &= 1 \qquad \text{if } x \geq 0 \\ &= 0 \qquad \text{if } x < 0 \end{aligned} \qquad (3\text{-}12)$$

$$\text{STEP (x,y)} = \int_{-\infty}^{x} \delta(x')\,dx' = \int_{-\infty}^{x} \text{line}\,(x')\,dx' \qquad (3\text{-}13)$$

If T is the linear transform of the imaging system,

$$\begin{aligned} \text{ERF (x)} &= \text{T [STEP (x,y)]} = \text{T} \left[\int_{-\infty}^{x} \text{line}\,(x')\,dx'\right] \\ &= \int_{-\infty}^{x} \text{T [line}\,(x')\,dx'] = \int_{-\infty}^{x} \text{LSF}\,(x')\,dx' \qquad (3\text{-}14) \end{aligned}$$

so that the LSF is the derivative of the ERF.

$$\text{LSF} = \frac{d}{dx}[\text{ERF(x)}] \qquad (3\text{-}15)$$

Therefore, the Fourier transform of the derivative of the ERF yields the MTF in one dimension according to equation (3-11).

$$\text{F}\left[\frac{d}{dx}[\text{ERF(x)}]\right] = \text{F [LSF(x)]} = \text{MTF}\,(u,0) \qquad (3\text{-}16)$$

There is a relationship of these three functions which can yield the MTF.

$$\int_{-\infty}^{\infty} \text{PSF (x,y)}\,dy = \text{LSF(x)} = \frac{d}{dx}[\text{ERF(x)}] \qquad (3\text{-}17)$$

3-3 Crosstalk

3-3-1 Background

Two waves in a dielectric waveguide can be coupled so effectively that complete transfer of power from one wave to the other is possible. This type of coupling results from a sinusoidal imperfection of the core-cladding boundaries or a sinusoidal variation of the index of refraction. The coupling of guided modes of two different waveguides is also possible and is based on the crosstalk phenomenon. The mode coupling between different waveguides is caused by imperfections in the waveguide geometry or by inhomogeneities of the dielectric medium of the waveguide (Marcuse 1972).

The transmitted image through an image guide can be blurred by mode coupling which is caused by crosstalk between pairs and between arrays of cylindrically symmetric or slowly varying fibers. The phenomenon of optical crosstalk between cores of fibers blur the transmitted image of the optical fiber bundle and lowers the resolution of the image guide. If one fiber of an image guide is excited, the electromagnetic fields of a fiber extend indefinitely and interact with any fibers which are around the first fiber. Figure 3-3 shows this crosstalk phenomenon in fiber optic image guides. Light illuminates the center fiber core and Figure 3-3-(a) shows a higher degree of crosstalk than Figure 3-3-(b).

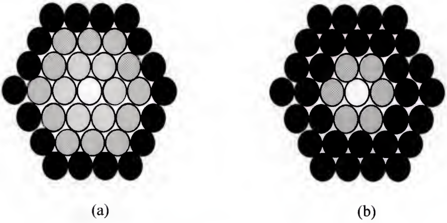
(a)

(b)

Figure 3-3 Schematic illustration of crosstalk phenomena. Only the center fiber is illuminated and surrounding fibers look partially illuminated due to crosstalk to a different degree in the two bundles.

This interaction excites the fields in surrounding fibers, which in turn interact with the fields of the first fiber. The overlap of the fields between fibers can determine the amount of crosstalk or power exchange which is associated with frustrated total internal reflection or equivalently, optical tunneling (Snyder and Love 1983). Therefore, the crosstalk phenomenon is very difficult to analyze by geometrical optics, and electromagnetic wave theory should be employed to analyze the crosstalk phenomenon (Yamaguchi et al. 1989).

The crosstalk phenomenon is observable by transmitting a sharp image through the image guide. Generally, the transmitted image will become blurry because crosstalk makes the output intensity decrease in the transverse direction. It is well known that crosstalk is a function of many variables including the fiber material, dimension and the numerical aperture of the optical fiber. Crosstalk of the image guide decreases when increasing the fiber center to center distance or the diameter of individual fibers, and when increasing the numerical aperture of the fibers. Also, crosstalk is increased when the length of image guide is increased and relates to fiber defects, such as the "shading or stain looking" image bundle (Huang et al. 1995). Recently, a new class of crosstalk in image fiber was studied experimentally (Komiyama and Hashmoto 1994). Komiyama et al. defined a new kind of crosstalk as the background crosstalk to distinguish it from the local crosstalk which is a general phenomenon. In their study, a new type of crosstalk was found in the background of the image transmitted through an image fiber. This background crosstalk should decrease with the fiber length because the guided core modes contribute to a wide spread of leakage and the powers of the modes are absorbed into the low refractive index coating around each microfiber (Komiyama and Hashmoto 1994).

Crosstalk is related to the modulation transfer function (MTF). This can be shown with the visual observation of image bundles. The image bundle with less crosstalk shows a higher MTF value and a sharper image (Huang et al. 1995, Kapany 1968). In addition, cross talk is strongly dependent on the order of guided modes in the image fiber and wavelength of visible light (Yamaguchi et al. 1989). Generally, the higher order modes give rise to crosstalk and the lower order modes contribute to transmission of the image through the optical fiber bundle (Komiyama and Hashmoto 1994). Generally, crosstalk becomes more severe for longer wavelengths. It is necessary to eliminate higher mode components in the input image to decrease crosstalk because the effect of higher modes upon crosstalk are very strong, especially, for short length fibers.

3-3-2 Characterization of Crosstalk

Many theoretical models and concepts have been developed to calculate and verify the amount of crosstalk and to understand the phenomenon itself. The elementary plane wave concept of frustrated total internal reflection was investigated to describe crosstalk between parallel, multimode waveguides or lightguides by Kapany and Burke (Kapany 1968). However this method is tedious and inapplicable to long multimode fibers. Also, crosstalk was described by the summed effect of coupled modes by Snyder and McIntyre (Snyder and McIntyre 1976). This method used mode theory to provide the first electromagnetic treatment of crosstalk between lightguides of circular cross section.

For an image guide, Hosono treated the phenomenon of cross talk between cores using the weak coupling theory (Hosono 1983). In his study, he shows the crosstalk increases exponentially in the packing ratio. The weak coupling approximation is adopted because the crosstalk is very weak in practical cases and the electromagnetic fields are approximated by scalar fields. Subsequently, the full wave theory was developed to analyze the transmission characteristics of image fiber with a one dimensional structure (Yamaguchi et al. 1989). In those papers, there were two limiting cases were considered. The first one was the crosstalk between lower order modes in a long image fiber and the other case was the crosstalk between higher order modes in a short image fiber. The leakage phenomenon was not considered in both cases. Komiyama and Hashimoto presented a two-mode coupling theory to describe the crosstalk and compared with experimental results. It has been shown that crosstalk occurs due to two different kinds of coupling. One causes the crosstalk to increase with the fiber length and the other causes the crosstalk independent of the fiber length (Komiyama and Hashimoto 1989). Another experimental research on image quality of an ultrathin needle scope was done by Fugikura Ltd. in Japan (Tsumanuma et al. 1989). They found that the image quality strongly depended on the suitable structure to the fiber length exists for the image fiber. And they considered both crosstalk and leaky rays which will be discussed in detail later to characterize the image quality of ultrathin needle scopes. It has been shown that the crosstalk between pixels is more severe in the case of a long image guide (1 m) than that of a short image guide (10 cm) and the amount of leaky ray is more in a short image guide (10 cm) compared to a long image guide (1 m). Therefore, the leaky rays can be a major factor which may deteriorate image quality in a short image guide less than 10 cm and the crosstalk can deteriorate image quality in a 1m long image guide.

To minimize crosstalk many methods have been developed in fabricating step index image guides. Fundamentally, if the thickness of cladding is increased, crosstalk should be reduced and if adjacent cores made dissimilar, crosstalk is also decreased (Arnaud 1976). However, if only cladding is thickened, definitely image brightness is decreased and if cladding thickness is increased at the same core-cladding ratio, the core center to center distance (pitch length) is longer. The longer pitch length automatically produces a low resolution image guide.

Since, crosstalk is not simple and can not be simply related to structure parameters but also material parameters of optical fiber, it is very difficult to define the amount of crosstalk between even two fibers. For many years, the theoretical approaches to obtain the amount of crosstalk has been studied. Generally, the coupling coefficient which is related to the amount of crosstalk can be defined according to the refractive index profile of the optical fiber. For step index profile fiber, the coupling coefficient (*C*) is given by the following equation (Snyder and Love 1983, Tsumanuma et al. 1989).

$$\mathrm{C} = \frac{u^2}{\mathrm{V}^3} \, \frac{\sqrt{2}\,(n_{co} - n_{cl})^{1/2}}{\rho \; n_{co}^{1/2}} \, \frac{\mathrm{K}_0(w\,d/\rho)}{\mathrm{K}_1^2(w)} \qquad (3\text{-}18)$$

where V is called the normalized frequency and is defined as,

$$\mathrm{V} = \frac{2\pi\rho}{\lambda}\sqrt{(n_{co}^2 - n_{cl}^2)} = \frac{2\pi\rho}{\lambda}\,\mathrm{NA} \qquad (3\text{-}19)$$

This V value is one of the most important parameters in fiber-optic communication system theory (Mclintyre 1973) as well as in fiber optic imaging (Kapany 1968). It consists of fiber core diameter, refractive index difference between core and cladding, vacuum wavelength and the distance between two adjacent pixels. In equation (3-18), ρ is the core radius, and d is the distance between two adjacent pixels. The k, u, w and β are wave number, modal parameters of the core and cladding and propagation constant, respectively.

$$k = \frac{2\pi}{\lambda} \tag{3-20}$$

$$u = \rho (k^2 n_{co}^2 - \beta^2) \tag{3-21}$$

$$w = \rho \ (\beta^2 - k^2 n_{cl}^2) \tag{3-22}$$

Also, K_0 and K_1 are modified Bessel function of the second orders of the 0 and 1.

For Gaussian profile fibers, coupling coefficient can be given by following equation (Snyder and Love 1983).

$$C = \left(\frac{\pi \Delta}{d \rho}\right)^{1/2} V^3 \frac{(V-1)^{1/2}}{(V+1)^{1/2}} \exp\left\{(V-1)\left[\frac{V-1}{V+1} - \frac{d}{\rho}\right]\right\} \tag{3-23}$$

where Δ is the profile height parameter and defined as,

$$\Delta = \frac{1}{2}\left\{1 - \frac{n_{cl}^2}{n_{co}^2}\right\} \cong \frac{n_{co} - n_{cl}}{n_{co}} \tag{3-24}$$

With a given value of coupling coefficient, the amount of crosstalk P_n is represented by the following equation for the single fiber illumination in an infinite one-dimensional array.

$$P_n(z) \cong J_n^2(2Cz) \tag{3-25}$$

where z is the fiber length, J_n is Bessel function of the first kind and n is the order from illuminated fiber as shown in Figure 3-4.

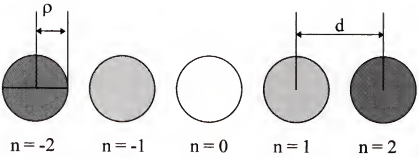

Figure 3-4 Infinite one-dimensional array of fibers labelled by n and with center to center distance, d, and core radius, ρ.

Figure 3-4 shows the crosstalk phenomenon in an infinite one-dimensional array of fibers and the light is illuminated only on the center fiber which is labeled by n = 0. Here, another term, beat length, Z_b, is introduced to explain crosstalk phenomenon. The beat length is defined as that distance along the waveguide in which there is total transfer of power from one fiber to the other fiber and back again.

$$Z_b = \frac{2\pi}{C} \tag{3-26}$$

In equation 3-26, as the coupling coefficient increases, the beat length becomes shorter.

In this study, it is very important to find the relationship between the coupling coefficient and other measurable variables such as core diameter, center to center distance, vacuum wavelength and so on. For fundamental mode, two different values of coupling coefficient between two same fibers are calculated using equation 3-18 and 3-23. The ranges and typical values of input parameters used to calculate coupling coefficient are listed in Table 3-1.

Table 3-1 The ranges and typical values of input parameters which are used to calculate coupling coefficient in equations 3-18 and 3-23

Input Parameters	Input Parameter Range	Typical Value
Microfiber core radius	2.5 - 4.5 μm	2.5 μm
Center to center distance / Core diameter	1.8 - 2.2	2.0
Numerical aperture	0.2 - 0.4	0.23
Vacuum wavelength	0.35 - 0.7 μm	0.55 μm

Figure 3-5 through Figure 3-8 show the relationship between the coupling coefficient and the input parameters for the SI and Gaussian profile fibers. There is a decrease of the coupling coefficient of both fibers for increasing core diameter with fixed cladding thickness, the same numerical aperture and the same wavelength. These results are the same as that of crosstalk which is stated in section 3-3-1.

Although the calculated values were normalized to examine the trends between the coupling coefficient and other variables in both step index and Gaussian profile fibers as shown in Figure 3-5 through Figure 3-8, the absolute value of the coupling coefficient between two SI profile fibers is larger than that of Gaussian profile fibers.. Thus, it is expected that the coupling coefficient between SI fibers is larger than that of GRIN fibers because the Gaussian profile fiber can be regarded as a category of GRIN profile fibers. However, it is very difficult to determine crosstalk of an image guide which has about 5000-10,000 microfibers, by assessing coupling coefficient alone, since it depends on many other parameters such as the structure, material of image guide and the condition of input light.

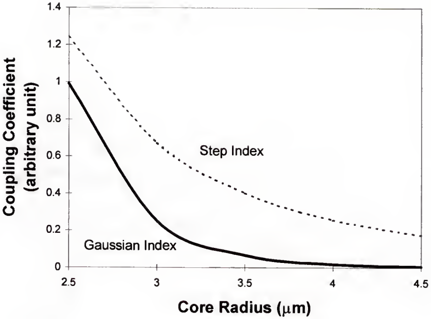

Figure 3-5 Coupling coefficient versus core radius in SI and Gaussian profile fibers with the same cladding thickness, wavelength, and numerical aperture

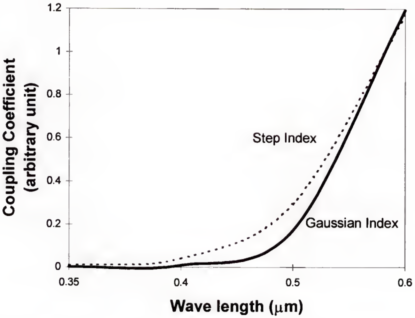

Figure 3-6 Coupling coefficient versus wavelength in SI and Gaussian profile fibers with the same core/cladding ratio, core diameter, and numerical aperture

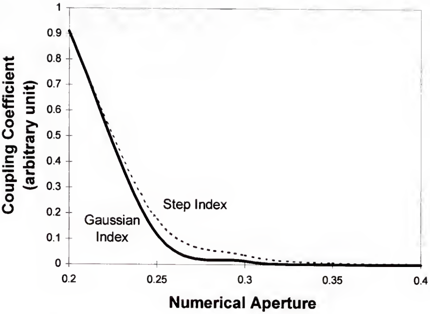

Figure 3-7 Coupling coefficient versus numerical aperture in SI and Gaussian profile fibers with the same core/ cladding ratio, core diameter, and wavelength

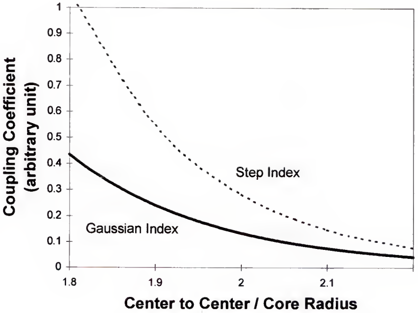

Figure 3-8 Coupling coefficient versus center to center / core radius in SI and Gaussian profile fibers with the same, core diameter, wavelength and numerical aperture

3-4 Leaky Rays

3-4-1 Background

In geometric optics, the ray tracing method using Snell's laws and Fresnel's reflection coefficients has long been accepted widely as a good approximation of the light acceptance and transmission properties of optical fibers, in cases where the ratio of fiber radius to wavelength is large (Kapany 1968). The geometric optics assumption is that if a ray satisfies the condition of total internal reflection, it is transmitted without any loss within an ideal fiber. In other words, if incident rays strike the fiber boundaries at angles equal to or greater than the critical angle, all the incident rays will be guided along the fiber without loss. However, a large class of rays are in fact attenuated in fibers with circular core section even though these rays are trapped and guided by total internal reflection according to geometric optics. This class of rays is defined as leaky rays and are distinguished from refracted rays that attenuate by the well-known mechanism of refraction (Snyder and Mitchell 1974). The most general description of leaky rays is that they are more skewed to the fiber axis than the bound rays which are guided along the fiber with satisfying the condition of the total internal reflection (Snyder et al. 1974). Subsequently, the rays in a circular shape optical fiber were classified into bound ray, tunneling ray and refracting ray. As a general term, leaky rays include refracting rays, tunneling rays in circular optical fiber (Snyder and Love 1974) and tunneling-refracting rays in noncircular optical fiber (Love et al. 1979). The tunneling rays are defined as the rays that appear to tunnel a finite distance into the cladding and they are associated with frustrated total internal reflection.

These leaky rays or leaky modes also play a role in the fiber core to deteriorate image quality of the fiber optic image guides. They move across the bundle, leaving one core and reaching another core, possibly at a distant site. This long range coupling is expected to decrease the contrast which is a major factor in image quality. However its influence on the deterioration of the modulation transfer function (MTF) at higher frequency should be of minor importance, although it does play a significant role over the whole frequency range (Conde et al. 1994).

3-4-2 Characterization of Leaky Rays

Ray invariants

There are two kinds of rays which are guided in circular optical fiber. The rays which cross the fiber axis between reflection are known as meridional rays and rays which never cross the fiber axis are known as skew rays. Figure 3-9 shows these two types of ray paths within a circular step index optical fiber. A meridional ray shows a zig-zag path and a skew ray shows a helical path. In step index fiber, the meridional ray and skew ray can be characterized by angle θ and ϕ respectively. Both angles are spherical polar angles to the axial direction of the fiber and are related to the angle α which is between the incident and the normal ray as shown in Figure 3-10. The three direction angles are related by

$$\cos\alpha = \sin\theta \sin\phi \tag{3-27}$$

In Figure 3-10, the angle of incidence or reflection is α relative to the normal Y-axis and the incident or reflected ray makes angle θ with the Z-axis. Angle ϕ is defined between the path projection (OP) and X-axis in the cross-section of the fiber.

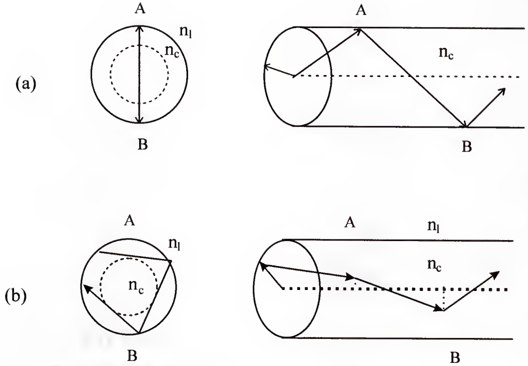

Figure 3-9 Two type of ray paths within circular step index fiber (a) meridional ray (b) skew ray

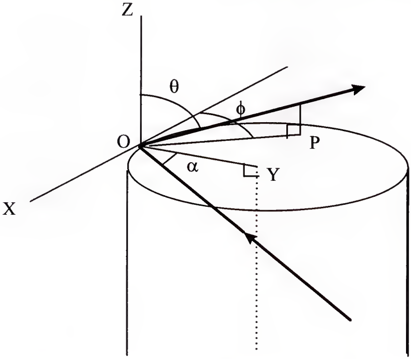

Figure 3-10 Angles for describing reflection of a ray incident at O in the case of step index fiber

By defining these angles, two different kinds of ray invariants can be introduced in step index fibers. The first invariant, β, accounts for the translational invariance of the fiber along its axis, and the second one, η, accounts for the azimuthal symmetry of the fiber.

$$\beta = n_{co} \cos\theta \tag{3-28}$$

$$\eta = n_{co} \sin\theta \cos\phi \tag{3-29}$$

$$\beta^2 + \eta^2 = n_{co}^2 \sin^2 \alpha \tag{3-30}$$

In graded index fiber, the meridional rays cross the fiber axis between successive turning points and skew rays follow a helical path such as the one of step index fiber. The ray invariants also can be defined in gradient index fibers.

$$\beta = n(r) \cos\theta(r) \tag{3-31}$$

$$\eta = \left(\frac{r}{\rho}\right) n(r) \sin\theta(r) \cos\phi(r)$$

$$= \left(\frac{r}{\rho}\right) \cos\phi(r) \left[n^2(r) - \beta^2\right]^{1/2} \tag{3-32}$$

where ρ is the core radius and the ray angles θ and ϕ are also defined in Figure 3-10. However, θ, ϕ and refractive index n are functions of radius, r, in gradient index fibers. These invariants β, η are determined by specifying r, θ, ϕ at any convenient point on the ray path. At radius r, θ(r) is the angle between the path tangent and the axial direction, and ϕ(r) is the angle in the core cross-section between the projection of the path tangent and the azimutal direction. If we eliminate θ(r) between the two equations 3-31 and 3-32, the skewness angle ϕ(r) is found and given in equation 3-33.

$$\cos\phi(r) = \frac{\rho}{r}\left(\frac{\eta}{\left[n^2(r) - \beta^2\right]^{1/2}}\right) \qquad (3\text{-}33)$$

It is noted that if $\phi(r) = \pi / 2$, η should be zero. Rays with η=0 have paths confined to a plane and are the meridional rays.

Classification of rays

The classification of rays in the optical fiber can be categorized by the ray invariants and refractive index. Generally, a refractive index profile can be defined as

$$\begin{aligned} n(r) &= n_{co} & 0 \le r < \rho \\ &= n_{cl} & r = \rho \end{aligned} \qquad \text{Step Profile} \qquad (3\text{-}34)$$

$$\begin{aligned} n(r) &= n_{co} & r = 0 \\ &= n_{co}(r) & 0 < r < \rho \\ &= n_{cl} & r = \rho \end{aligned} \qquad \text{GRIN Profile} \qquad (3\text{-}35)$$

where $$n_{co}(r) = n_{co}\left[1 - 2\Delta(r/\rho)^g\right]^{1/2} \qquad \text{g-profile} \qquad (3\text{-}36)$$

If all the gradient occurs at the interface, the step profile may be considered as the extreme limit of a gradient profile. Therefore, a general case of the classification for gradient profile fibers can be used for step index profile fiber (Snyder and Love 1983).

The general classifications of rays in GRIN and SI circular fiber are listed in Table 3-2. For step index fibers, the β_{min} and $\eta_{max}(\beta)$ in the category of tunneling rays become 0 and $[n_{co}^2 - \beta^2]^{1/2}$, respectively as the value of g in equation 3-36 increases to infinity.

Table 3-2 The general classification of rays in GRIN and SI circular fiber

Bound rays	$n_{cl} < \beta \leq n_{co}$
Refracting rays	$0 \leq \beta^2 + \eta^2 < n_{cl}$
Tunneling rays	$\beta_{min} \leq \beta < n_{cl}$ and $n_{cl}^2 - \beta^2 \leq \eta^2 \leq \eta_{max}^2(\beta)$

where

$$\begin{aligned} \beta_{min} &= 0 & : n_{co}^2 \geq n_{cl}^2 \frac{(g+2)}{g} \\ &= [\, n_{cl}^2 - (g/2)(\, n_{co}^2 - \, n_{cl}^2)]^{1/2} & : n_{co}^2 \leq n_{cl}^2 \frac{(g+2)}{g} \end{aligned} \tag{3-37}$$

$$\eta_{max}(\beta) = g^{1/2} [\frac{2}{n_{co}^2 - \, n_{cl}^2}]^{1/2} [\frac{n_{co}^2 - \, \beta^2}{g+2}]^{(g+2)/2g} \tag{3-38}$$

The criteria of the tunneling rays for step index profile fibers may be simplified as

$$n_{cl}^2 \leq \beta^2 + \eta^2 \leq n_{co}^2 \qquad \text{and} \qquad 0 \leq \beta < n_{cl} \tag{3-39}$$

Figure 3-11 shows a schematic distribution of rays on circular step index (SI) and graded index (GRIN) fibers according to the value of the invariants β and η (Snyder and Love 1983). In Figure 3-11, BR, TR and RR represent bound ray, tunneling ray and refracting ray, respectively. It is of great interest to compare the schematic ray distribution of step index fiber with that of GRIN fiber because the tunneling ray may have deleterious effects on fiber optic imaging where the main source of error is the leaky ray. It is easily found in Figure 3-11 that in the GRIN fiber, there are relatively fewer tunneling rays than in step index fiber. There are analytic approaches by which one can calculate the ratio of tunneling to bound ray power (Ankiewicz and Pask 1977). The g factor in the g-profile and Gamma functions are used to represent the ratio of tunneling to bound ray power.

$$\frac{P_{tr}}{P_{br}} = \frac{g+2}{g}\left\{\frac{g+4}{g+2} - \sqrt{\pi}\frac{\Gamma[(g+2)/2]}{\Gamma[(g+3)/2]}\right\} \tag{3-40}$$

$$= \frac{1}{3} \qquad g = 2 \text{ (parabolic profile)}$$

$$= 1 \qquad g = \infty \text{ (step index profile)}$$

where the subscripts *tr* and *br* refer to tunneling and bound rays, respectively. For parabolic GRIN fibers, if the value of g equals 2, the ratio of P_{tr} / P_{br} is 1/3. For step index profile (g=infinite), the P_{tr}/P_{br} is 1. Thus, in the GRIN fiber, there are relatively few tunneling rays than in the SI fiber (Ankiewicz and Pask 1978).

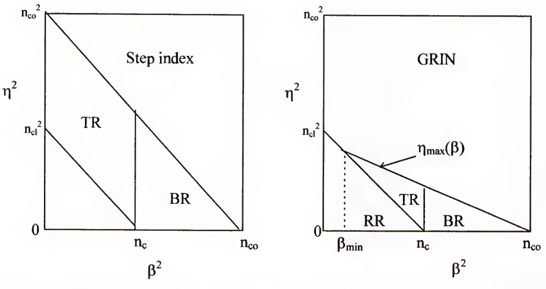

Figure 3-11 Schematic distribution of rays on circular step index and graded index optical fibers

3-5 Summary

In this chapter, the image assessment methods in fiber-optic imaging system were discussed. Especially, the modulation transfer function (MTF) is described in detail. This method is generally used to decide the image quality in various kinds of medical imaging systems as well as in fiber-optic imaging systems. In Chapter 6, this MTF will be obtained by measuring edge response function (ERF) of a sharp image to characterize image quality of the plastic GRIN image guides and image plates.

The critical phenomena which deteriorate image quality in fiber-optic imagery were discussed. Especially, crosstalk and leaky rays are the major factors to make image quality worse in ultrahigh resolution fiber-optic imagery. Although, the theoretical or experimental studies of both phenomena have not been completed in fiber-optic imaging till now, the leaky ray effect deteriorates image quality in short length image guides and crosstalk plays a significant role to deteriorate image quality in long length image guides.

It was shown theoretically that the coupling coefficient between two SI profile fibers is larger than that of Gaussian profile fibers. Although the crosstalk is related to the coupling coefficient, it is very difficult to determine crosstalk by assessing only the coupling coefficient because crosstalk depends on many other parameters such as the structure, material of image guide, and the conditions of input light.

In addition, the tunneling rays which are the components of the leaky rays in GRIN fiber are less than those of SI fiber. For the parabolic (g-value = 2) in g-profile GRIN fiber, the ratio of tunneling ray power to bound ray power is 1/3, and in SI fiber, the power ratio of tunneling to bound ray power is 1. Therefore, it is expected that the image quality of ultrahigh resolution (less than 5 μm microfiber diameter) GRIN image guide is better than that of SI image guide because crosstalk and leaky ray effects become severe as the diameter of microfiber is made smaller than 5 μm.

CHAPTER 4
FABRICATION OF PLASTIC GRADED INDEX IMAGE GUIDES FOR ULTRAHIGH RESOLUTION ENDOSCOPES

4-1 Introduction

In the last decade, remarkable progress has been made in the development of ultrathin endoscopes (Tsumanuma et al. 1989). Figure 4-1 shows the structure of an ultrathin endoscope image guide.

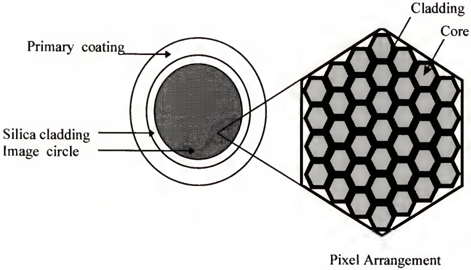

Figure 4-1 Schematic structure of ultrathin endoscope image guide

The hexagonal array of 2000 fibers are made from step index glass optical fiber. A step index (SI) optical fiber is one in which a fiber is composed of a core glass surrounded by a cladding glass where the refractive indices are n_1 and n_2 ($n_1 > n_2$), respectively. Light at greater than the critical angle, which is transmitted down the core glass suffers internal reflection with almost 100% efficiency at the core/cladding interface. Although the light reflects efficiently at the boundary, a small fraction of the light enters the cladding before reentering the core. If the cladding is not quite thick enough, some light may leak through the cladding into the adjacent fiber. This causes a reduction in resolution, and reduction in contrast sensitivity. If the core diameter is reduced, at fixed cladding thickness, less light is transmitted and the image loses brightness. Hence, there is an optimum fiber core diameter, and cladding thickness for a given microfiber size. This optimization process has been studied experimentally by Tsumanuma (Tsumanuma et al. 1988).

Figure 4-2 shows the modulation transfer function of the image guide versus frequency for different cladding thicknesses at fixed microfiber diameter (5 μm). The result is that maximum resolution (MTF) is achieved with a core diameter equals 3 μm, and radial cladding thickness of 1 μm, i.e. core/cladding = 3.0.

They also measured the MTF of ultrathin image guides which have different core size with optimum core/cladding ratio (Tsumanuma et al. 1988). Figure 4-3 shows the MTF of image guides with different microfiber diameter from 5 μm to 2 μm which have the same numerical aperture and same core/cladding ratio of 3. In Figure 4-3, the image guide with 5 μm microfiber diameter (i.e. 3 μm core diameter and 1μm cladding thickness) shows maximum resolution even though it has the largest core diameter of the four kinds of image guides. As described in Chapter 3, the crosstalk and leaky rays make spatial resolution lower in SI image guides which have microfiber diameters less than 5 μm.

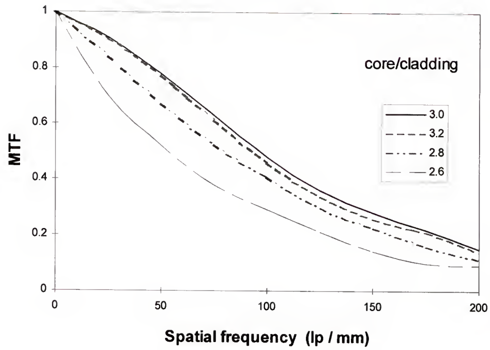

Figure 4-2. Modulation transfer function versus frequency of SI ultrathin image guides with different core/cladding ratio

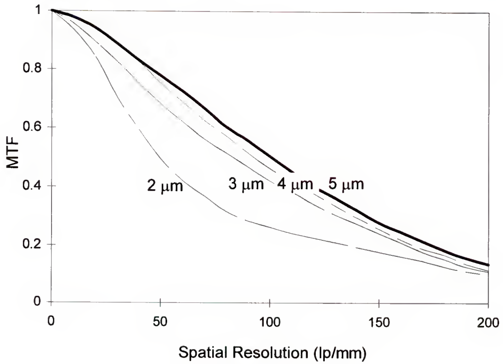

Figure 4-3 Measured spatial resolution of glass step index image guides (NA = 0.43, core diameter/cladding thickness = 3)

With optimum dimensions of core and cladding, only 36% of the light which hits the end of the image guide actually strikes the area defined by the cores of the microfibers. Most of the available light is lost on the cladding area. Figure 4-4 illustrates this problem. Since only the light striking the core area can contribute to image brightness, it is clear that only a marginal reduction in microfiber diameter can be made while pursuing higher resolution.

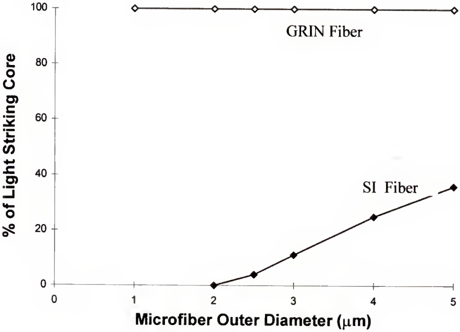

Figure 4-4. Percent of light striking microfiber core area which closely related to image brightness versus microfiber outer diameter

It may be concluded, that the existing technology of ultrathin endoscopes have hit a limit. The diameter of the presently employed microfibers cannot be reduced in size due to diminishing image brightness, and the resolution of ultrathin endoscope cannot be further improved using the existing conventional techniques. However, it is possible to obtain higher resolution and brighter image guide with GRIN fibers because the percent of light striking microfiber core area is not changed in GRIN fiber even below 5 μm microfiber outer diameter as shown in Figure 4-4.

4-2 Preparation of GRIN Preforms

As discussed in Chapter 2, MMA-BMA system was used to polymerize GRIN preforms by interfacial-gel copolymerization method. Before polymerization, both monomers, MMA and BMA were distilled to get rid of any impurities. Bubbles can be caused by any impurities in the monomers during polymerization and make the transmittance of preforms (polymeric rods) decrease. The properly chosen chain transfer agent (CTA) and initiator also should be filter-cleaned and used in appropriate amount. The CTA plays an important role to determine polymer molecular weight which has an effect on the flexibility of the plastic optical fiber (POF). The polymerization starts with the help of an initiator which controls the speed of polymerization as well as the degree of polymerization.

Distilled MMA-BMA monomer mixture, CTA and initiator were placed in a PMMA tube which was thoroughly cleaned and dried for 2-3 days in the vacuum oven. The PMMA tube filled with monomer mixture in the glass tube was heated in an oil bath.

The copolymerization starts at the PMMA tube side because a gel phase was formed at the interface of monomer mixture and PMMA tube. Due to the "gel-effect," the copolymerization rate in the gel phase is much faster than that of the liquid phase. Therefore, the copolymerization process progresses radially inwards to the axis. Figure

4-5 shows the processes of the interfacial-gel copolymerization technique and refractive index profiles of produced copolymers.

The mechanism of interfacial-gel copolymerization is different from that of polymerization. Copolymerization requires different monomer reactivity ratios (r_1, r_2) of two kinds of monomer. The reactivity ratio of one monomer (r_1) should be greater than 1 and that of the other monomer (r_2) should be less than 1. In this case the MMA reactivity ratio is 0.93 and the BMA reactivity ratio is 1.05 (Koike et al. 1991). Since the composition of produced copolymer depends on monomer reactivity ratio, the copolymer at large radius at the PMMA tube side has much more MMA than BMA and the copolymer along the axis contains a large amount of BMA. A gradient index profile is formed according to the composition of copolymer because the refractive indices of the two homopolymers are different from one another (PMMA : 1.49, PBMA :1.568).

As listed in Table 4-1, it was very difficult initially to obtain bubble free GRIN preforms. The polymerization temperature, time and the amount of initiator were the critical factors to cause bubbles during polymerization process. Bubbles can be caused by the impurities in the monomer mixture or by dust in the polymerization environment. Another possibility to cause bubbles is a fast reaction process. Thus, the monomer mixtures were distilled and kept in the refrigerator in the bottles with sealing caps. Additionally, the polymerization processes were carried out in a class 1000 clean-room to prevent dust from causing bubbles and reducing transmission of the preforms. Since, the reaction rate depends on the initiator and the conditions of polymerization such as time and temperature, the choice of initiator was very important to obtain bubble free preformed rods. As a initiator, Lauroyl peroxide of which 10hrs half-life temperature is 62 ^{O}C was used.

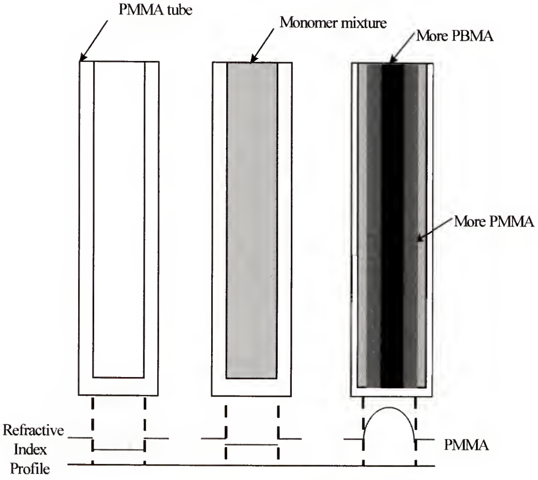

Figure 4-5 Schematic diagram of interfacial-gel copolymerization with MMA/BMA mixture

Table 4-1 The compositions and conditions of copolymerization for GRIN preforms

	Monomer Mixture	Initiator (wt. %)	CTA (wt. %)	Conditions (temp./time)	Bubbles	Result
1	MMA/BMA 3/1	0.1 % LP	0.2 % Octanethiol	75 °C / 72 hrs 90 °C / 24 hrs	many in / out	X
2	MMA/BMA 4/1	0.1 % LP	0.2 % Octanethiol	75 °C / 72 hrs 90 °C / 24 hrs	a few out side	Δ
3	MMA/BMA 5/1	0.1 % LP	0.2 % Octanethiol	75 °C / 72 hrs 90 °C / 24 hrs	a few in / out	Δ
4	MMA/BMA 4/1	0.1 % LP	0.2 % Octanethiol	75 °C / 72 hrs 100 °C / 36 hrs	a few out side	Δ
5	MMA/BMA 4/1	0.3% LP	0.2 % Octanethiol	75 °C / 72 hrs 100°C / 36 hrs	many in / out	X
6	MMA/BMA 4/1	0.5% LP	0.2 % Octanethiol	75 °C / 72 hrs 100 °C / 36 hrs	many in / out	X
7	MMA/BMA 5/1	0.1 % LP	0.4% Octanethiol	75 °C / 72 hrs 100 °C / 36 hrs	a few in / out	X brittle
8	MMA/BMA 5/1	0.1% LP	0.2 % Octanethiol	75 °C / 72 hrs 100°C / 36 hrs	a few in / out	Δ flexible
9	MMA/BMA 5/1	0.1% LP	0.1% Octanethiol	75 °C / 72 hrs 100 °C / 36 hrs	a few in / out	Δ flexible
10	MMA/BMA 4/1	0.1 % LP	0.2% Octanethiol	85 °C / 72 hrs 130 °C / 24 hrs	many in / out	X
11	MMA/BMA 4/1	0.2% LP	0.2 % Octanethiol	85 °C / 72 hrs 130°C / 24 hrs	many in / out	X
12	MMA/BMA 5/1	0.1% LP	0.2% Octanethiol	85 °C / 72 hrs 130 °C / 24 hrs	many in / out	X

Table 4-1 continued

	Monomer Mixture	Initiator (wt. %)	CTA (wt. %)	Conditions (temp./time)	Bubbles	Result
13	MMA/BMA 4/1	0.1 % LP	0.2% Octanethiol	60 °C / 24 hrs 75 °C / 48 hrs 110 °C / 24 hrs	a few outside	Δ
14	MMA/BMA 4/1	0.1% LP	0.2 % Octanethiol	60 °C / 24 hrs 75 °C / 48 hrs 110 °C / 24 hrs	a few outside	Δ
15	MMA/BMA 4/1	0.1% LP	0.2% Octanethiol	60 °C / 24 hrs 75 °C / 48 hrs 110 °C / 24 hrs	a few outside	Δ
16	MMA/BMA 5/1	0.1 % LP	0.2% Octanethiol	65 °C / 20 hrs 85 °C / 40 hrs 120 °C / 12 hrs	a few in / out side	Δ
17	MMA/BMA 5/1	0.1% LP	0.2 % Octanethiol	65 °C / 20 hrs 85 °C / 40 hrs 120 °C / 12 hrs	a few in / out side	Δ
18	MMA/BMA 4/1	0.1% LP	0.2 % Octanethiol	60 °C / 48 hrs 75 °C / 24 hrs 95 °C / 40 hrs 120 °C / 24 hrs	no bubbles	O
19	MMA/BMA 4/1	0.1% LP	0.2 % Octanethiol	60 °C / 48 hrs 75 °C / 24 hrs 95 °C / 40 hrs 120 °C / 24 hrs	3-4 bubbles	O

LP : Lauroyl Peroxide
Results : X (cannot be used), Δ (may be used), O (can be used)

4-3 Verification of GRIN Properties

After obtaining bubble free GRIN preforms, it is necessary to verify that the preform has a radial GRIN profile. Although the best method is to measure the refractive index profile of the drawn fiber, this method is very difficult and needs very accurate optical instruments. However, there are two simple methods to find GRIN properties. The first method is to examine beam trajectories within a GRIN preform using a laser. The laser beam should travel in a curved path in the GRIN preform. In this case, the face of the preform should be well polished to reduce any scattering from the face except Fresnel's reflection. Figure 4-6 shows the proof of GRIN characterization of the preform using a He-Ne laser beam (630 nm wavelength).

The second method is to obtain an image through a GRIN preform or fiber. A radial GRIN preform has a unique characteristic which can focus light, so it can be used as a lens. The image through a cylindrical GRIN preform can be erect or inverted according to its length. Figure 4-7 shows the inverted and erect images through GRIN lenses of whose pitch lengths are 0.25 and 0.75, respectively.

It is possible to determine the physical length of the cylindrical GRIN lens according to the pitch with the maximum, minimum refractive indices, and the radius of the cylindrical object. The refractive index distribution in a radial gradient objects is given as

$$n(r) = n_o\left(1 - \frac{\left(\sqrt{A}\, r\right)^2}{2}\right) \tag{4-1}$$

In equation (4-1), if r = 0, then n(0) = n_o and if r = R, then n(R) = n_R. Where n_o, n_R are the maximum and minimum refractive indices and R is the radius of the cylindrical GRIN object. The term $\sqrt{A}$ is the gradient constant and defined as,

$$\sqrt{A} = \left\{ \frac{2(n_o - n_R)}{n_o R^2} \right\}^{1/2} \tag{4-2}$$

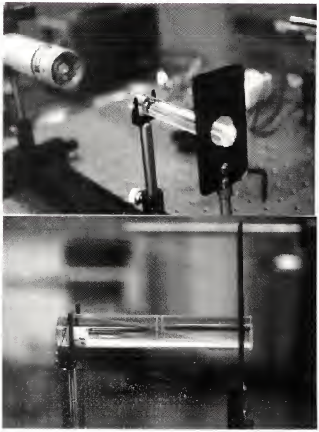

Figure 4-6 Laser beam trajectory method to examine GRIN property. Upper picture shows He-Ne laser setup and next picture shows curved beam through the GRIN preform

There is a relationship between the gradient constant and the pitch of the GRIN object. i.e.,

$$2\pi \; P = \sqrt{A}\, Z \tag{4-3}$$

where P and Z are the pitch and the physical length of the cylindrical GRIN object, respectively.

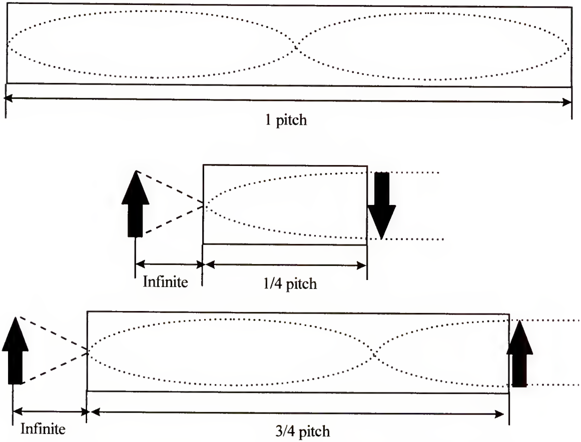

Figure 4-7 The inverted and erect images through a cylindrical GRIN lens which has radial gradient index profile

From the equation (4-2) and (4-3), the physical length can be determined as,

$$Z = \sqrt{2}\pi \ PR\left\{\frac{n_o}{(n_o - n_R)}\right\}^{1/2} \tag{4-4}$$

Therefore, the physical length of the cylindrical GRIN lens for a given pitch length can be measured to deduce the GRIN properties.

In this study, the GRIN preforms and fibers were examined to verify GRIN properties. Using equation 4-4, the physical length of GRIN objects according to pitches, 0.25 and 0.75, were determined to obtain the inverted and the erect images, respectively. However, the GRIN lens should be cut 3-5mm longer than the desired physical length which was determined by equation 4-4, because polishing is needed on both end-surfaces of GRIN lens. Table 4-2 lists measured physical lengths of GRIN preform and fiber which have an inverted image.

Table 4-2 The lengths of GRIN preform and fiber which have an inverted image

GRIN	Pitch	n_o	n_R	R	Z	Image
Preform	0.25	1.53	1.49	17.5 mm	120 mm	Inverted
Fiber	0.25	1.53	1.49	0.5 mm	3.4 mm	Inverted

In the case of 1mm diameter GRIN fiber, the inverted image was obtained at 3.4 mm length fiber and the erect image also captured at 10.2 mm length fiber as expected.

4-4 Fabrication of GRIN Image Guides

To fabricate an ultrahigh resolution GRIN image guide, a multiple drawing method was used. Figure 4-8 shows a schematic sequence of the triple-drawing process. The whole process was done in a class 1000 clean-room in order to avoid contamination. First, a strand of round GRIN optical fiber (Figure 4-8-(a)) was produced by drawing a preform GRIN rod using a drawing tower.

Figure 4-9 shows a schematic diagram of the drawing process. To obtain uniform diameter fibers, the drawing tower is operated and controlled by a computer program. The main parameters which affect a fiber diameter are boule size and shape, heater temperature, boule feed rate and fiber take-up speed. The computer is made to control only the fiber take-up speed which is adjusted depending upon the drawn fiber diameter which is measured by Laser Mike (fiber diameter gauge) as shown in Figure 4-9. Usually, the fiber shape, heater temperature and boule feed rate were fixed before drawing. Thus, an initial good guess of the fixed values is very important to achieve stable control of the drawing tower. Figure 4-10 shows the flow chart of the fiber drawing control system.

The drawn fibers were cut to a fixed length. The equal length fibers were then square-stacked in a square metal fixture and subsequently fused together in a vacuum oven (Figure 4-8-(b)). The boule of (N x N) array of fused plastic optical fibers was then placed in the heated enclosure of the draw tower with a nitrogen environment where its tip softens and a fiber was once more drawn down and cut at proper lengths (Figure 4-8-(c)).

These second drawn multi-fibers were then square-stacked (M x M) in a square cross-section fixture and subsequently fused together in a vacuum oven once more (Figure 4-8-(d)). The resulting boule of ((N x N) x (M x M)) array of fused optical fibers was drawn down again to make a final multi-multi optical fiber. Usually, the third drawing is under the same processing conditions as the first and second drawing. The multi-multi optical fiber has $(N \times M)^2$ image transmitting elements (Figure 4-8-(e)). For example, if N=M=10, the multi-multi optical fiber has 10,000 image transmitting elements. For N=M=32, the number of image transmitting elements exceeds 1,000,000. Fibers of this type may be used for the production of endoscopes or boroscopes. It is also possible to go one additional step and fabricate an ultrahigh resolution fused image plates. In this case, one more fusing process is required. Figure 4-8-(f) shows a fused image plate.

4-4-1 First Drawing, Stacking, and Fusing

The heater temperature was 540 ^{o}C and the oxygen level was 0.2% at the first drawing. The fiber take-up speed and the boule feed rate are about 2.2 m/min and 10mm/min respectively. The drawn fiber diameter was 1 mm and the diameter uniformity was held to better than ± 5%. The accuracy can deteriorate if bubbles are present inside the preform. Bubbles inside the preform can cause severe problems in the drawing process such as irregularity of target fiber diameter and even fiber breakage. Thus, a bubble-free preform is the first requirement to obtain uniform diameter fiber which is essential for effect uniform packing in the stacking process.

The 1.0 mm diameter fiber is cut into 25 cm lengths, and 625 of them are bundled together in a 25 x 25 square array. This boule is contained in a 25 mm x 25 mm cross-section aluminum square fixture. The fixture is placed in a heated vacuum oven at 125 °C for 2.5 hrs to make a fused boule of solid polymeric fibers.

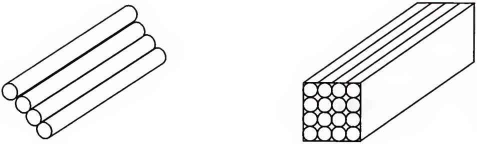

(a) First drawn and cut to single fibers

(b) First stacked and fused single fibers

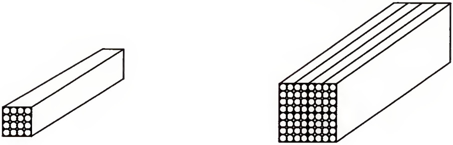

(c) Second drawn multi-fiber

(d) Second fused multi-fibers

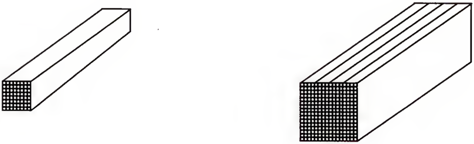

(e) Third drawn multi-multi fiber
(Ultrahigh resolution image guide)

(f) Third fused multi-multi fibers
(Ultrahigh resolution fused image plates)

Figure 4-8 Schematic diagram of multiple-drawing process for the ultrahigh resolution image guides and fused image plates

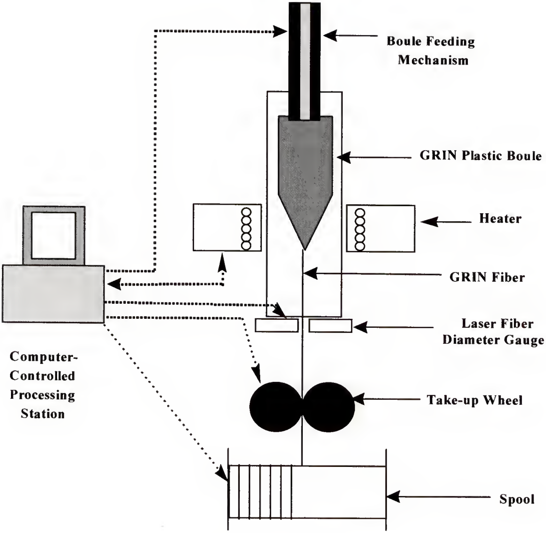

Figure 4-9 Schematic diagram of drawing tower

4-4-2 Second Drawing, Stacking, Fusing, and the Final Drawing

The conditions of the second drawing, fusing are the same as those of the first process. The size of the second drawn square fiber is 1 mm x 1 mm and the multi-fiber contains 40 μm microfibers. These multi-fibers are cut to 20 cm lengths and 100 of them are bundled together coherently in a 10 x 10 square fixture. The fixture is again placed in a vacuum oven until fusing is complete. The fused boule is placed in the oven in the draw tower.

The heater temperature of the third drawing is the same as in the previous drawings (540 °C). The final multi-multi fibers are drawn with outer diameters of 1.25 mm, 1.0 mm, 0.75 mm and 0.5 mm containing microfibers of 5 μm, 4 μm, 3 μm and 2 μm in diameter, respectively. Figure 4-11 shows the cross-section of the GRIN image guide with 3 μm microfiber diameter.

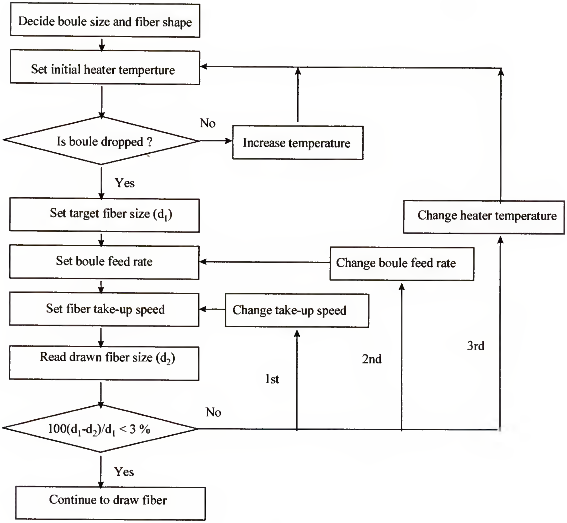

Figure 4-10 The flow chart for the fiber drawing control system

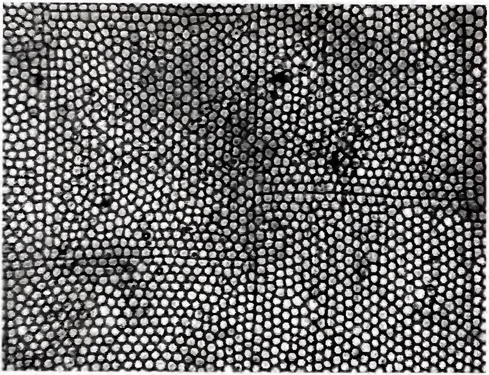

Figure 4-11 The cross-section of the GRIN image guide with 3 μm microfiber diameter (1000X magnification)

4-4-3 Special Clean Stacking Process

All the processing of drawing, stacking and fusing are carried out in a class 1000 clean-room, to minimize the many tiny dust particles which can reduce the transmission of plastic optical fiber. If the final microfiber size is 50 μm, dust less than 10 μm does not much affect the transmission of the fiber. But in the case of 2 μm microfiber diameter image guide, even 5 μm size dust can block a few pixels of the image guide. Therefore, a special clean stacking process is needed to obtain high quality ultrahigh resolution fiber-optic image guide. The process is :

- Examine the cut fiber using a 10X eyepiece. If there is a black or other color foreign object, discard the fiber. It could be dust which came from the drawing process.

- Collect the cut fibers and place in an ultrasound cleansing bath for 5-10 minutes. The solution to be used is filtered and distilled water.
- Take the wet fiber out of the bath and place on a stainless steel plate which should have a polished, clean surface and electrically grounded.
- Place the fiber in a one dimensional array and discard any fiber with obvious defects.
- Lay the fibers side by side to make one layer, then place scotch tape at both ends of the layer and wrap it around the layer.
- The taped layer of fiber is then placed in the cleansing bath for further cleaning.
- When enough layers are made, prepare the lay-up fixture. The fixture requires Teflon sheet between the fiber array and the metal fixture. Also measure the dust particle level during the assembly procedure. It is important that the whole fiber boule assembly should be build as quickly as possible to minimize dust contamination by the surrounding air.
- Take a layer of fiber out of the bath and remove any water using compressed air. The air line should have a fine particle filter (<0.1 μm) to prevent any contamination by the compressed air.
- The dried layer of fiber is placed in the fixture carefully, and gently blow clean, ionized air over the layer of the fibers, which will have some surface charge build up by the action of placing the layer in the fixture. Use a static charge sensor to verify the neutralizing action.

- Once a N x N array of fibers or multi-fibers is stacked, place a cover lid to secure the boule by tightening bolts firmly.
- The boule assembly should be vacuum dried at 70 °C for at least 24 hrs in the clean-room.

4-5 Summary

The ultrahigh resolution (less than 5 μm) plastic GRIN image guides were fabricated successfully. The preforms are produced by the interfacial-gel copolymerization technique with MMA/BMA monomer mixture system. As listed in Table 4-1, there were many trials to find the conditions which result in bubble-free preforms.

The GRIN preform was tested to verify the GRIN properties. After first drawing, the plastic GRIN fiber is also tested using the inverted-erect image checking method described in section 4-3.

The transmission of the image guides which have more than 50 μm microfiber diameter are not much affected by the residual dust in the class 1000 clean-room. However, the dust is the most critical factor to deteriorate the transmission of ultrahigh resolution image guide which has less than 5 μm microfiber diameter. Therefore, a new cleaning procedure is necessary to fabricate an ultrahigh resolution image guide even in the class 1000 clean-room. This procedure was described in section 4-4-4. The optical qualities which include the image brightness and the resolution of the plastic GRIN image guides will be characterized in the following chapter.

CHAPTER 5
FABRICATION OF ULTRAHIGH RESOLUTION PLASTIC GRADED INDEX IMAGE FACEPLATES

5-1 Introduction

A fiber-optic element is an optical device made of a bundle of optical fibers each having a very small (a few micron) diameter. The element transfers an image with high efficiency and low distortion. Use of such an element can make an optical design simple, ragged and compact because there is no need to consider the use of an optical lens. Fiber-optic elements include fused plates, image conduits, fiber-optic tapers, image guides, and image inverters. Especially, fiber-optic fused plates are defined by solid coherent bundles in which the bundle length is shorter than the bundle cross-sectional dimension. Typical applications for fused plates are charge coupled device (CCD) windows faceplate, image intensifiers, and camera tube faceplate (Allan 1973).

The aim of this chapter is to describe the fabrication of an ultrahigh resolution (below 5 μm pixel element) plastic graded index fiber-optic fused plates for imaging. Existing fused plates have traditionally been made from glass SI optical fibers with optimized refractive indices depending on the application. The resolution of glass SI fiber optic plates is limited to about 5 μm and the glass fused fiber-optic plate is heavy due to the high density (2.4 g/cm^3) of glass.

To fabricate an ultra-high resolution (below 5 μm) image plate, gradient index plastic optical fibers can be used because GRIN fiber has many advantages over SI fiber as described in section 1-3.

As stated in Chapter 2, there are different techniques to make plastic GRIN material. The first one is the interfacial-gel polymerization techniques (Ishigure et al. 1994) with additives whose radial distribution is controlled to produce the required refractive index profile. Another technique is interfacial-gel copolymerization (Koike 1988, Ohtsuka et al. 1990) of two monomers with different refractive indices, whose relative concentrations vary radially to produce the required refractive index profile.

The thermal processes such as drawing and fusing have to be carried out three times to make a high resolution image fused plate. In particular, temperature and processing time are the most critical parameters during the thermal processes of GRIN material which are made using the interfacial-gel polymerization technique because additives in the GRIN fibers can rapidly diffuse out in the high temperature processing time. But, in the case of GRIN material using interfacial-gel copolymerization, there is no degradation of the profile in high temperature because the polymers have no chance of diffusion.

In this study, two kinds of plastic GRIN rods were prepared by using the two different techniques; interfacial-gel polymerization and copolymerization. The first technique failed due to additive migration during the multiple thermal processing steps required to produce the fused image plates. The ultrahigh resolution fused image plates were able to be successfully made using only copolymerized GRIN fibers.

5-2 Preparation of GRIN Preforms

Although, methyl methacrylate (MMA) and benzyl methacrylate (BMA) were selected to copolymerize GRIN preforms in Chapter 2, another copolymer made of methyl methacrylate (MMA) and vinyl benzoate (VB) is used to copolymerize GRIN preforms for the image plates.

It is expected that MMA/VB system has a higher numerical aperture than that of MMA/BMA system because the refractive index of poly-VB is higher than that of poly-BMA. Table 5-1 lists the refractive indices and the numerical apertures of both systems.

Table 5-1 The refractive indices and numerical apertures of MMA/BMA and MMA/VB monomer mixture systems

Refractive Index of Polymer		Refractive Index of Copolymer		Effective Numerical Aperture
PMMA	1.490	80% PMMA + 20% BMA	1.506	0.265
PBMA	1.568	20% PMMA +80% BMA	1.552	
PVB	1.578	80% PMMA + 20% VB	1.508	0.282
		20% PMMA +80% VB	1.560	

As listed in Table 5-1, MMA/VB system has higher numerical aperture than MMA/BMA system. But the transmittance of MMA/VB system is worse than that of MMA/BMA system. In fabricating image faceplates, numerical aperture is more important parameter than the transmittance of copolymer, since the thickness of the image plate is usually less than a few centimeters. So, MMA/VB system is more suitable for plastic fused image plates.

The procedure of copolymerization of MMA/VB system is almost the same as that of the MMA/BMA system as described in section 4-2. The conditions such as copolymerization temperature and time, the amount of initiator and chain transfer agent are listed in Table 5-2. After GRIN preforms were obtained, the characterization process was carried out by the same methods as described in section 4-3.

Table 5-2 The compositions and conditions of copolymerization for GRIN preforms

	Monomer Mixture	Initiator (wt. %)	CTA (wt. %)	Conditions (temp./ time)	Bubbles	Transmission	Result
1	MMA/VB 5/1	0.03% BBMB	0.2 % GDMA	70 °C / 17 hrs 90 °C / 72 hrs	a few in / out	bad (yellow)	X
2	MMA/VB 5/1	0.03% BP	0.2 % GDMA	70 °C / 17 hrs 90 °C / 72 hrs	a few out side	bad (yellow)	X
3	MMA/VB 5/1	0.5% BP	0.2 % GDMA	70 °C / 17 hrs 90 °C / 72 hrs	a few in / out	very bad (amber)	X
4	MMA/VB 3/1	0.05% BP	0.2 % GDMA	45 °C / 24 hrs 70 °C / 48 hrs 90 °C / 24 hrs	many in / out	bad (yellow)	X
5	MMA/VB 4/1	0.05% BP	0.2 % GDMA	45 °C / 24 hrs 70 °C / 48 hrs 90 °C / 24 hrs	a few in / out	bad (yellow)	X
6	MMA/VB 5/1	0.05% BP	0.2 % GDMA	45 °C / 24 hrs 70 °C / 48 hrs 90 °C / 24 hrs	a few in / out	bad (yellow)	X

Table 5-2 Continued

	Monomer Mixture	Initiator (wt. %)	CTA (wt. %)	Conditions (temp./ time)	Bubbles	Transmi-ssion	Result
7	MMA/VB 4/1	0.2% BP	0.2 % GDMA	65 °C / 20 hrs 90 °c / 48 hrs 110 °C / 20 hrs	many in / out	good (clear)	X
8	MMA/VB 4/1	0.1% BP	0.2 % GDMA	45 °C / 24 hrs 70 °C / 48 hrs 90 °C / 24 hrs	many in / out	good (clear)	X
9	MMA/VB 4/1	0.05% BP	0.2 % GDMA	45 °C / 24 hrs 70 °C / 48 hrs 90 °C / 24 hrs	a few in / out	good (clear)	Δ
10	MMA/VB 4/1	0.05% BP	0.2 % GDMA	45 °C / 24 hrs 90 °C / 56 hrs	a few in / out	good (clear)	Δ
11	MMA/VB 4/1	0.05% BP	0.2 % GDMA	65 °C / 18 hrs 90 °C / 48 hrs 110 °C / 15 hrs	a few out side	good (clear)	O
12	MMA/VB 4/1	0.05% BP	0.2 % GDMA	65 °C / 18 hrs 90 °C / 30 hrs 110 °C / 24 hrs	a few out side	good (clear)	O

BBMB : Bis[1-(tert-butylperoxy)-1-methylethyl]benzene
BP : Butane Peroxide
GDMA : Glycol Dimercaptoacetate
Result : X (cannot be used), Δ (may be used), O (can be used)

The optimum compositions and conditions of copolymerization of a MMA/VB system are listed in the last parts of Table 5-2. Because the transmission of a preform which is copolymerized using the MMA/VB system is worse than that with the

MMA/BMA system, the selection is based on not only bubbles in the preform but also the color of the preform.

5-3 Fabrication of Plastic GRIN Fused Image Faceplates

Figure 4-8 shows the multiple drawing processes of the ultrahigh resolution fused image plate which is completed by the third fusing process (Figure 4-8-(f)).

Figure 5-1 shows the transmitted image of a 1 cm thick plastic GRIN fused fiber-optic image plate with 400X magnification. The average diameter of each fiber is about 5 μm. The image transmission quality of GRIN image plates will be described in Chapter 6.

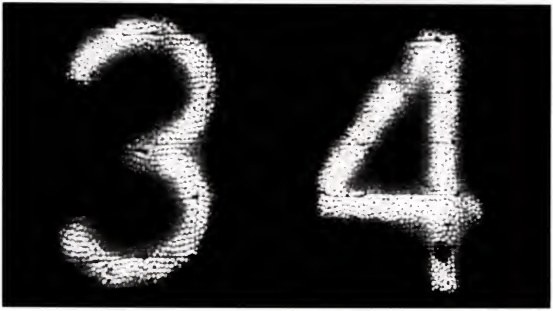

Figure 5-1 The transmitted image of a plastic GRIN image plate with 5 μm diameter microfibers (400X magnification)

5-4 Special Absorbent Material

It is necessary to discuss special absorbent material which maybe placed inside of the image plate, although it is not used in this study. Usually, the special absorbent material is added in the fabrication of SI fiber-optic image plates. If the numerical aperture of the input light is higher than that of the fibers, the light which is not accepted by the fibers can cause a serious reduction in the contrast and resolution of the final image. This effect can be reduced by use of special absorbent material. There are three ways in which the absorbent material can be added.

One is the extra-mural absorption (EMA) method which is the obvious one of surrounding each fiber by a second cladding of absorbing material. The light within the numerical aperture of the fiber is almost reflected from the first cladding which is a transparent. And, the stray light which penetrates the first cladding is absorbed by the second cladding. These stray light rays, i.e., leaky rays as described in Chapter 3, can cause severe reduction of the image quality in the fiber-optic fused plates.

The second method to reduce stray light is the interstitial technique. In this method, the special absorbent material is introduced into the stack in the form of rods which are placed in the interstitial voids between the fibers.

The last method is to use the dead single type absorbent material. The absorbent material which has the same diameter as a single optical fiber is arranged in each multi-fiber bundle as though it is a transmitting fiber. Although, the modulation transfer function and resolution performance of this method is not as good as EMA or the interstitial technique, the ease of assembly makes it attractive for many fiber-optic manufacturers. Figure 5-2 illustrates the EMA, interstitial and dead single type techniques.

Although, all three methods to absorb the stray light are useful to increase the image quality of the fused image plates, they have some disadvantages First, the fabrication process with absorbent material is complicated. Second, the fabrication cost should be higher and third, by using absorbent material, the packing fraction can be reduced and the brightness of fused image plate is reduced. Additionally, the dead single fiber can be considered to be a blemish which is a small area (spot or line) within the fiber optic assembly with reduced transmission.

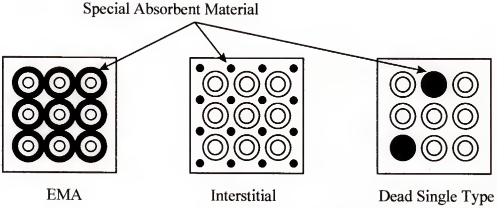

Figure 5-2 Three methods in which the special absorbent material can be added

When the EMA technique is used, variations of core packing fraction plotted as a function of microfiber diameter are shown in Figure 5-3. In the case of a SI fiber, the cladding thickness is 1 μm, and the EMA thickness is taken to be 0.5 μm in both SI and GRIN fibers. It is apparent that a GRIN based plate can function better than a SI plate for fiber diameter less than 5 μm.

It is expected that the special absorbent material is more necessary for SI fused image plate than GRIN one, because there are relatively more tunneling rays which are in the category of leaky rays in SI fiber than in the GRIN fiber as described in Chapter 3.

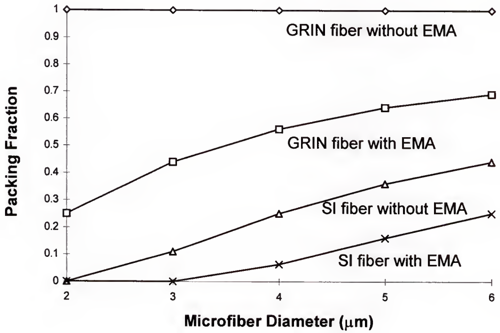

Figure 5-3 Variation of core packing fraction plotted as a function of microfiber diameter with EMA

5-5 Summary

The ultrahigh resolution fused image plates were fabricated with plastic GRIN fibers. The GRIN preforms were made from the MMA/VB system to get a higher numerical aperture than is possible from the MMA/BMA system. The multiple drawing method which is explained in Chapter 4 is used to make microfiber diameters smaller than 5 μm. The manufacturing process of the image plates is the same as those of the image guide except for the third fusing process. Although, special absorbent material has not been used in fabricating the GRIN fused image plates described in this dissertation, it is discussed in the last part of this chapter because the EMA, interstitial, and dead single type techniques are essential to fabricate commercial SI fused image plates.

CHAPTER 6
OPTICAL CHARACTERIZATION OF ULTRAHIGH RESOLUTION PLASTIC GRADED INDEX IMAGE GUIDES AND IMAGE FACEPLATES

6-1 Introduction

As was discussed in Chapter 3, there are many parameters which can have an effect on the image quality in fiber-optic imaging system. These parameters can be divided into three main categories. The first category includes the structural parameters such as fiber diameter, fiber spacing between core center to center, the irregurity of fiber shape, imperfections and fiber length. The second category is referred to the material parameters such as numerical aperture of the fiber and attenuation coefficient. The last category includes system parameters such as the numerical aperture of the light source and its wavelength.

Although all these parameters are important to characterize the image quality of the fiber-optic system, it is difficult to characterize all these parameters separately. Therefore, there are a few methods to assess the overall image quality of the fiber-optic imaging system. As a typical method, the modulation transfer function (MTF) is used to characterize the image resolution and contrast.

In this study, the modulation transfer functions are obtained from the edge response functions (ERF) of the transmitted sharp images. The ERFs of the transmitted image through image guides and image plates were measured by different optical setups.

In addition, the image brightness of the image guide is obtained by measuring the numerical aperture and the attenuated power of the image guide. These results are compared with the published data of the glass SI image guides

6-2 Optical Characterization of Ultrahigh Resolution Plastic Graded Index Image Guides

6-2-1 Image Brightness

As described in section 1-3-2, the brightness, B, of the transmitted image by a guide is defined as (Wang et al. 1995) :

$$B = PF\,(NA)^2\,10^{-\left(\frac{\alpha L}{10}\right)} \qquad (1\text{-}7)$$

where PF is referred to as the packing fraction, which is defined as the ratio of the area of the core to the total area of the fiber. In the case of GRIN fiber, the PF always equal to 1 because there is no cladding, and the PF of the SI fibers are listed in Table 1-2 for different microfiber diameters. The PF depends on the cladding thickness which affects the image quality.

Measurement of numerical aperture (NA)

To measure the NA of GRIN image guide, a projection method was used. As shown in Figure 6-1, if a laser beam is launched into the one end of fiber with a beam diffuser, a circular intensity distribution is observed a few inches away from the other end of the fiber due to the diverging beam exiting the fiber. The angular dimension of this pattern gives the numerical aperture of the optical fiber. A beam diffuser is placed at the entrance of the fiber to ensure that the laser beam overfills the angular phase space.

The numerical aperture of the image guide is defined as the angle in radian between the beam axis and the edge of projected image as shown in Figure 6-1. Thus the NA can be determined by using the following formula:

$$NA = \tan^{-1}\left[\frac{D}{2S}\right] \tag{6-1}$$

where D is the diameter of the beam pattern and S is the distance from the end of the image guide to the optical detector. Since these two values should be measured very accurately, the value of D was determined by measuring 5 % of maximum transmitted power at the edge of circular beam distribution and the distance S can be measured exactly on the optical table. Figure 6-2 shows the transmitted power distributions of the plastic GRIN and glass SI image guides. The measured data and resultant numerical apertures of both image guides are listed in Table 6-1.

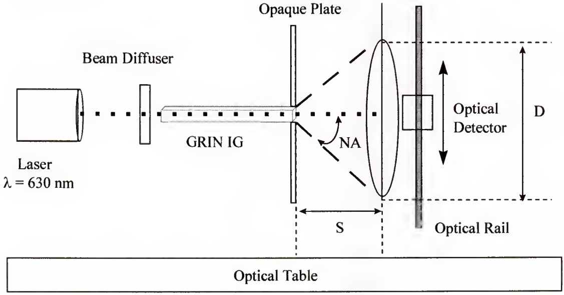

Figure 6-1 Numerical aperture measurement setup

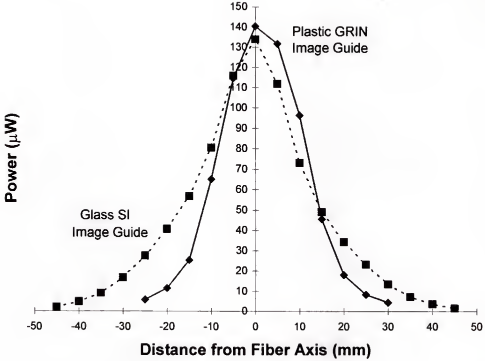

Figure 6-2 The transmitted power distributions of plastic GRIN and glass SI image guides

Table 6-1 Numerical aperture measurements of plastic GRIN and glass SI image guides

	S (cm)	D (cm)	NA
Plastic GRIN Image Guide	10.16	4.85	0.23
Glass SI Image Guide	10.16	6.90	0.33

As listed in Table 6-1, the resultant numerical apertures of plastic GRIN image guide is in the range of 0.23 and that of glass SI image guide is 0.33.

Measurement of attenuated power ratio

The attenuation coefficient, α, can be measured by the conventional cut-back method as a function of wavelength as given in equation 6-2 (Costa and Sordo 1981).

$$\alpha_{db} = \frac{10}{(L_1 - L_2)} \log_{10}\left(\frac{P_2}{P_1}\right) \tag{6-2}$$

where L_1 and L_2 are the original and cut-back fiber length respectively, and P_1 and P_2 are the corresponding output optical powers at a specific wavelength from the original and cut-back fiber length. However, the cut-back method is useful in the case where there is a significant difference between L_1 (typically 1-2 m) and L_2 (typically 1-2 km) for optical fibers used in communications. Since, it was not permissible to obtain long lengths of image guide, the attenuated power ratio (APR) of a given length of image guide was measured using the following equation.

$$APR = \frac{P_2}{P_1} = 10^{-\left(\frac{\alpha L}{10}\right)} \tag{6-3}$$

This measured APR of given length of the image guide can be used directly in equation 6-3. The APR measurement setup is shown in Figure 6-3. Light at 665nm from a light emitting diode (LED) is injected into a launching fiber whose diameter and numerical aperture are equal to or smaller than any image guide to be studied. The light intensity power at the exit of the launching fiber is measured with a photodiode in the power meter as shown in Figure 6-3.

The measured attenuated power ratio of equal length of glass SI and plastic GRIN image guides with various microfiber size are listed in Table 6-2. The length of the plastic image guides was chosen to be 310mm in order to compare with the same available length of glass SI image guide. The results are listed in Table 6-2.

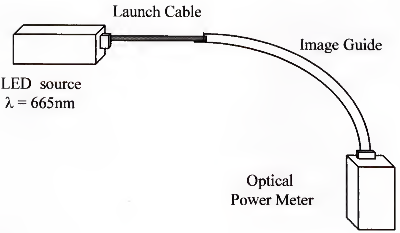

Figure 6-3 Experimental methods for measuring attenuated power ratio through an image guide

To establish a baseline for the image guide transmission measurements, an initial measurement was made with a fiber which has excellent transmission. The fiber chosen for this purpose was a 0.75 mm diameter Mitsubishi single core plastic optical fiber whose specified and measured attenuation was 180 dB/km (0.18 dB/m). Thus, for a distance of 310 mm, this fiber could be considered to have zero attenuation. This fiber was inserted between the exit of the launch fiber and power meter. In Table 6-2, the value of α = 25.0 dB/m was calculated based on the measured power. Since the fiber is assumed to have zero attenuation, this finite value of α was produced by several factors: coupling losses between the launch fiber and the Mitsubishi fiber, Fresnel light losses at the exit of the Mitsubishi fiber, and coupling light losses between the exit of the Mitsubishi fiber and the light sensitive diode of the power meter. The baseline attenuation of α = 25 dB/m should be subtracted from the measured value of a for any image guide fiber which is inserted as a replacement of the Mitsubishi fiber. The final results for attenuation of the image guides after subtraction of the 25 dB/m are given in

Table 6-2. The attenuation coefficient of plastic image guide below 3 μm diameter microfiber could not be compared with glass SI image guides because of its unavailability.

Table 6-2 The attenuated powers and attenuation coefficients of glass SI and plastic GRIN with different microfiber size

	Mitsubishi	Glass SI		Plastic GRIN			
Microfiber Diameter (μm)	0.75mm Single Fiber	4.1	3.1	4.1	3.1	2.4	1.8
Measured APR	0.282	0.138	0.091	0.141	0.105	0.072	0.023
Measured α (dB/m)	25.1	30.1	32.8	30.0	32.0	34.1	39.2
Normalized α (dB/m)		5.0	7.7	4.9	6.9	9.0	14.1

From Table 1-2, 6-1, and 6-2, the parameters and measured values are assembled in Table 6-3 to obtain the image brightness of the image guides.

Table 6-3 The parameters and measured values to obtain the image brightness of the glass SI and plastic GRIN image guide with different microfiber size

	Microfiber Diameter	PF	NA	APR	Image Brightness
Glass SI	4.1	0.44	0.33	0.138	0.0066
	3.1	0.44	0.33	0.091	0.0044
Plastic GRIN	4.1	1.0	0.23	0.141	0.0075
	3.1	1.0	0.23	0.105	0.0055
	2.4	1.0	0.23	0.072	0.0038
	1.8	1.0	0.23	0.023	0.0012

The image brightness of both SI and GRIN image guides with different microfiber size are shown in Figure 6-4. At the same microfiber size and same numerical aperture, the image brightness of plastic GRIN image guide is higher than that of glass SI image guide.

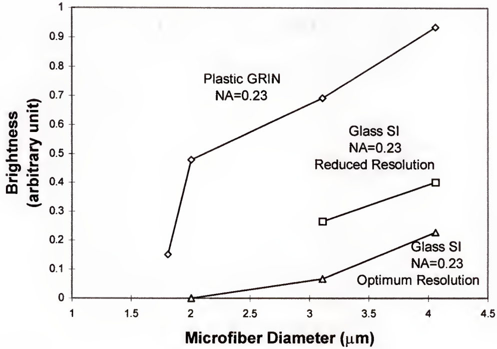

Figure 6-4 The measured image brightness of the plastic GRIN and glass SI image guides with the same microfiber outer diameter and numerical aperture. The cladding thickness of the reduced resolution SI image guide is less than 1μm and that of optimum resolution SI image guide is 1μm

In this figure, the packing fractions of the reduced resolution SI image guides are 0.44 and those of the optimum resolution SI image guides are 0.24, 0.11 and 0 according to microfiber outer diameter, 4 μm, 3 μm and 2 μm, respectively. As described in Chapter 1, the image brightness of SI image guides are deteriorated severely below 4 μm microfiber outer diameter because the cladding thickness should be at least 1 μm to obtain the optimum resolution. For the reduced resolution SI image guides in which cladding thickness is less than 1 μm, the image brightness is improved but still inferior to that of plastic GRIN image guides.

6-2-2 Image Resolution

The sharpness of the transmitted image is measured in the conventional way by studying the edge of an object.

An optical positioning table, rail and posts are used to measure the edge response function (ERF) of the transmitted image of the GRIN image guide as shown in Figure 6-4. As a target image, the USAF 1951 resolution target is used. A light source (Xe light source, Olympus Inc.) illuminates a sharp edge placed in direct contact with the polished surface of the image guide. The surface of the ultrahigh resolution image guide must be polished to within a few microns of surface roughness. The conventional polishing methods such as sand paper, polishing table and buffer wheel were not adequate to obtain a satisfactory polished-surface. Well polished surfaces of the plastic image guides were achieved by using a polishing machine (Microfin #140, PM MFG.Services Inc.). This machine is specially designed to polish the plastic material by cutting the surface 3-4 times with carbide and diamond cutters.

The output image from the proximal end of a 20 cm long image guide is read out by a 50X magnifying lens and a high resolution charge coupled device (CCD) camera system whose images are acquired by a Mac II based frame grabber as shown in Figure 6-5. Figure 6-6 shows the output image of the sharp edge transmitted by a GRIN image guide made of 3.5 μm diameter microfibers. The spatial resolution is investigated using the ERF. The ERF is the spatial intensity distribution across the image of an infinitely sharp edge. Figure 6-7 through Figure 6-10 shows the measured ERFs of the 7 μm, 5 μm, 3.5 μm and 2.5 μm microfiber diameter plastic GRIN image guides, respectively.

The magnification factor of the system is 2117 as described in Figure 6-5. In all of the Figures(6-7 through 6-10), a sharp change in the light distribution can be observed corresponding to the edge of the object. Systematic fluctuation in the light intensity over distances of a few microns can also be observed corresponding to light transmission through individual or small groups of fibers. It should be noted that the appearance of regions of zero light between fibers is due to the numerical aperture of a GRIN fiber of radius, *d*, being a sensitive function of radius, *r*:

$$NA\left(\frac{r}{d}\right) = NA\,(0)\sqrt{\left[1-\left(\frac{r}{d}\right)^{2}\right]} \tag{6-3}$$

As a result, the transmitted light intensity drops towards the outer boundary of a fiber as $[1-(r/d)^2]$. This gives the appearance seen in Figure 6-7 through Figure 6-10.

The digital data corresponding to Figure 6-7 through Figure 6-10 are used for the analysis of modulation transfer functions (MTF). Each of these sets of data are taken by averaging over a “swath” of fibers comprising 6 fibers by about 8 fibers in the case of the 5μm diameter fibers and corresponding by more for the smaller diameter fibers.

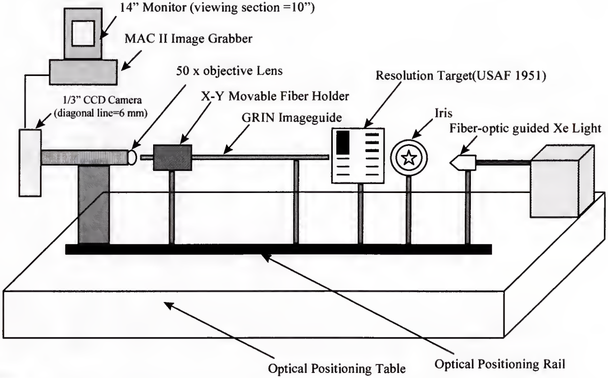

Magnification = microscope object lens x (monitor / CCD camera) =50 x (10 x 2.54) / 0.6 = 2116.7

Figure 6-5 ERF measurement setup

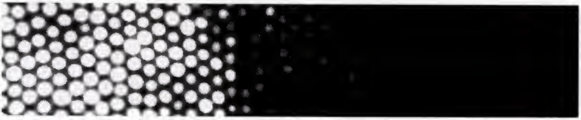

Figure 6-6 The output sharp edge image of the GRIN image guide with average 3.5μm diameter microfibers (2117X magnification)

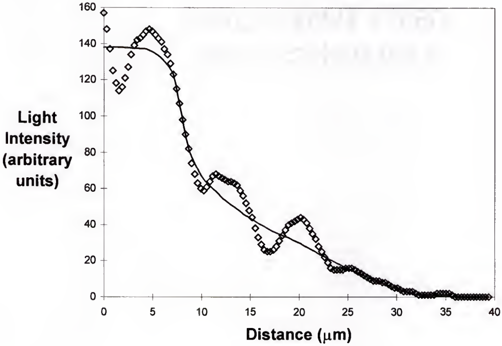

Figure 6-7 The measured edge response function of the plastic GRIN image guide with 7 μm diameter microfibers

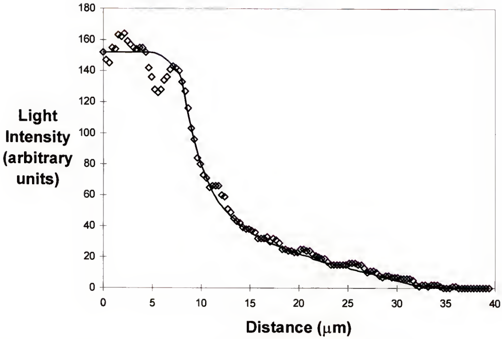

Figure 6-8 The measured edge response function of the plastic GRIN image guide with 5 μm diameter microfibers

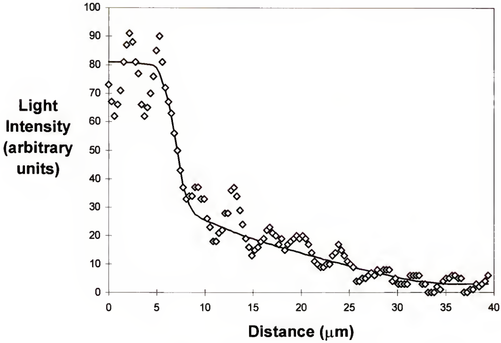

Figure 6-9 The measured edge response function of the plastic GRIN image guide with 3.5 μm diameter microfibers

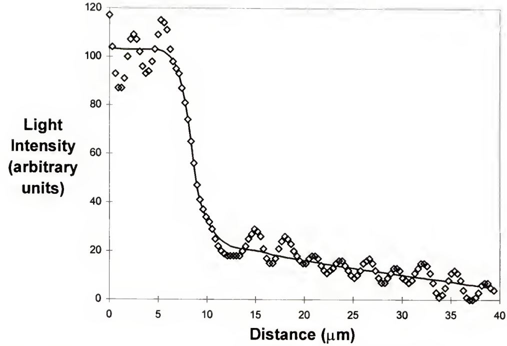

Figure 6-10 The measured edge response function of the plastic GRIN image guide with 2.5 μm diameter microfibers

Figure 6-11 shows how to obtain the digital data from the sharp edge image when the diameter of each fiber is 5 μm. The pixel size of the measuring system is 0.33 x 0.33μm^2 which can resolve the image of the ultrahigh resolution (2-5 μm) image guide. Each 8-bit digital data (128 gray levels) is obtained from averaging 100 pixel values. Thus, a 5 μm microfiber is mapped by 16.7 x 16.7 image pixels. The modulation transfer function (MTF) of the image guide is obtained from the Fourier transform of the line spread function (LSF) which is the derivative of the edge response function (ERF) as given in equation 3-16.

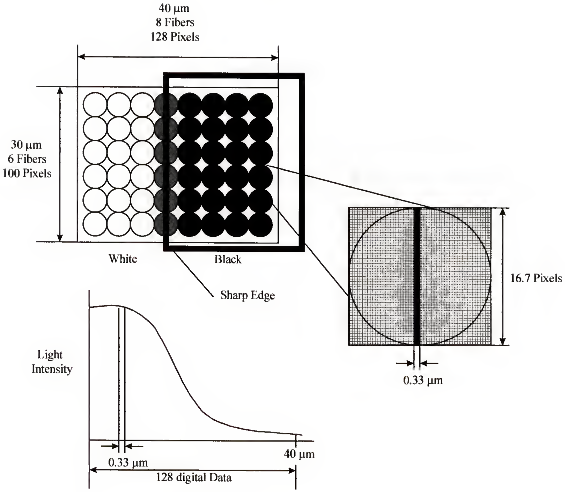

Figure 6-11 The method for obtaining the digital data from captured sharp image

The ERFs are obtained from the solid lines in the Figure 6-7 through Figure 6-10. The solid lines are best fits from the measured data. The resultant MTFs of the plastic GRIN image guides with different microfiber diameter, i.e., 7 μm, 5 μm, 3,5 μm and 2.5 μm are shown in Figure 6-12.

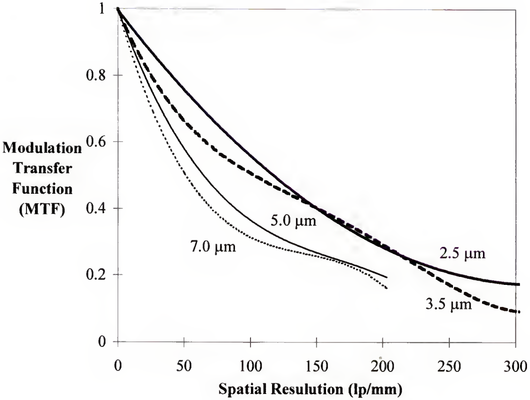

Figure 6-12 The modulation transfer functions of plastic GRIN image guides with different microfiber diameter size

The MTFs of the GRIN image guides are different from those of SI image guides as shown in Figure 4-3. The optimum resolution of the SI image guides was achieved when the diameter of the core is 3 μm, and the cladding thickness is 1 μm, (ratio of core/cladding equals 3.0). However, the GRIN image guide with 2.5 μm diameter microfibers has higher spatial resolution than those with 7 μm, 5 μm and 3.5 μm diameter microfibers as shown in Figure 6-12. Thus, it has been shown that the ultrahigh resolution image guides with less than 5 μm microfiber diameter can be achieved by only GRIN fibers.

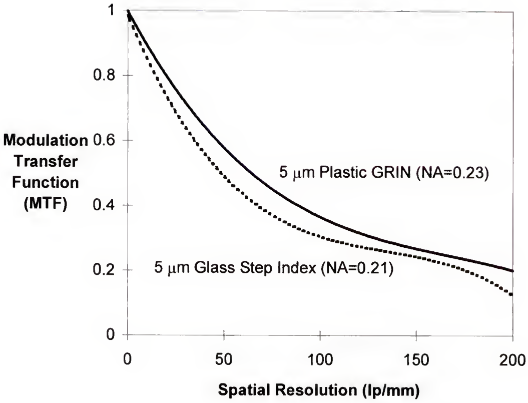

Figure 6-13 The modulation transfer functions of glass SI and plastic GRIN image guides with 5 μm microfibers

The measured MTF of the image guide with 5 μm plastic GRIN fibers was compared with the known data (Tsmanuma et al. 1988) of the same size of glass SI fibers as shown in Figure 6-13. In Figure 6-13, it is to be expected that the 5 μm plastic GRIN image guide has a MTF very similar to that of the glass SI image guide because of similar size microfibers and because the NA of both image guides because the numerical aperture (NA) of the SI image guide is 0.21 which is close to the NA of the GRIN image guide, which is 0.23. This conforms that the present measurement technique is reliable.

6-3 Optical Characterization of Ultrahigh Resolution Plastic Graded Index Fused Image Plates

6-3-1 Defects

A number of defects can occur in a fused image plate. These can be devided into blemishes and distortions.

Blemishes

Blemishes are defined as black areas where transmittance is less than 50% (Allan 1973). Usually, bubbles or dust which obstruct light transmission cause blemishes. The size of blemishes are indicated as the diameter of a circle equivalent to the surface area of the blemish. With a blemish size of *a* μm (vertical) by *b* μm (horizontal), the size of the blemish, S, can be defined as (Hamamatsu 1996)

$$a \times b = \pi \; r^2 \tag{6-4}$$

$$S = 2\,r = 2 \times \sqrt{\frac{a \times b}{\pi}} \tag{6-5}$$

Especially, the line blemish which occur along the border between multi-fibers (or multi-multi fibers) is called chicken wire. Generally, the chicken wire has a width equal to that of two or more microfibers. Most chicken wires are caused by partial breaks in the multi-fibers or multi-multi fibers. Equation 6-5 is also used to evaluate chicken wires in fused image plates.

In this study, dust caused blemishes in plastic GRIN image plate as shown in Figure 6-14. The black blemishes in the white image is surely dust which is obstructing the light transmission.

Distortions

When a fiber is out of position or bent in the manufacturing process, distortion can occur. There are three types of distortions such as shear, gross distortion and frame run-out. Shear distortion is seen by the discontinuity of a strait line image. Gross distortion makes the image of a straight line curved and is caused by the uneven flow of the multi-fibers during fusing process.

Figure 6-14 shows the shear distortion and blemishes of the GRIN image plate with 400X magnification. The straight line image looks distorted at the interface of multi-fiber bundles. The main reason for this phenomena is due to different microfiber size or multi-fiber bundle size.

Although frame run-out is also in the category of distortion, it differs from shear and gross distortions. Frame run-out often happens in the cutting process when the fibers are not normal to the end faces. Frame run-out tends to occur over the entire fused image plate.

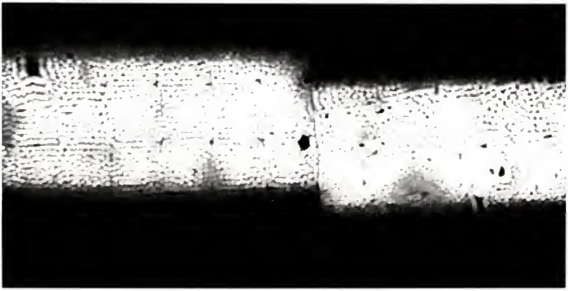

Figure 6-14 The shear distortion and blemishes of the GRIN image plate

6-3-2 Image Resolution

The general concept and method to measure edge response functions (ERF) of GRIN fused plates are the same as those used for image guides as described in section 6-2-2. However, the ERF measurement setup is different from that of image guides because of the short thickness of fused image plates.

Figure 6-15 shows the ERF measurement setup for plastic GRIN image plates. The magnification factor of the system was 2117. Figure 6-16 shows the sharp edge images of GRIN image plates with 5 μm and 2.8 μm diameter microfibers.

The measured ERFs of 5 μm, 2.8 μm and 2 μm fused image plates are shown in Figure 6-17 through Figure 6-19. The digital data corresponding to Figures 6-17 through 6-19 were obtained by the same method used in measuring the ERF of image guides as described in section 6-2-2. As shown in Figure 6-17 through Figure 6-19, the sharpness of the edge improves as the microfiber size decreases from 5 μm to 2 μm. However, the edge response of the 2 μm pixel image plate demonstrates a significant increase in the amount of light which leaks across the edge of the image. The MTFs of the 5 μm and 2.8 μm are analyzed using the solid lines shown in Figures 6-17 and 6-18, respectively. Figure 6-20 shows the MTFs obtained from 5 μm, 2.8 μm plastic GRIN image plates and 5 μm glass SI image plate.

The 5 μm plastic GRIN image plate has an MTF which is similar to that of the glass SI image guide. This similarity in resolution is to be expected because of the same microfiber diameter. When the 5 μm plastic image plate MTF data is compared with that from 2.8 μm plastic image plate. A major improvement can be seen in resolution for 2.8 μm compared to the 5 μm image plate. The difference in image resolution is large and consistent with the difference in microfiber diameter.

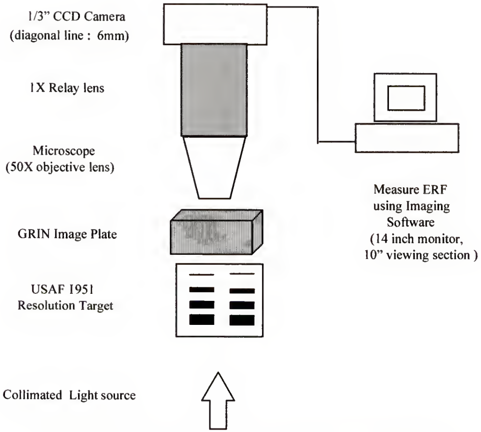

Magnification = microscope object lens x (monitor/CCD size)
= 50 x (10 x 2.54) / 0.6 = 2116.7

Figure 6-15 The edge response function measurement setup

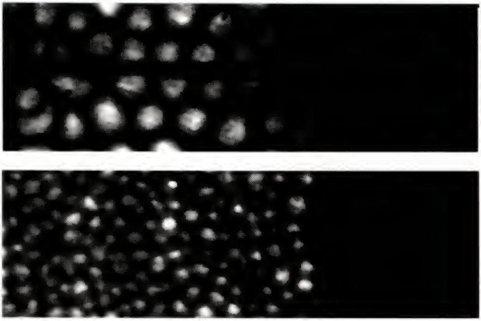

Figure 6-16 The sharp edge images of the GRIN image plates with different microfiber diameter 5 μm and 2.8 μm, respectively

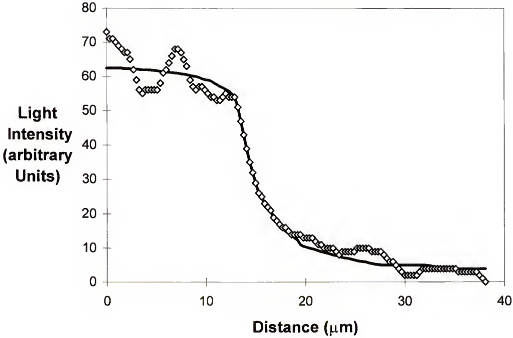

Figure 6-17 The measured edge response function of fused image plate with 5 μm diameter microfibers

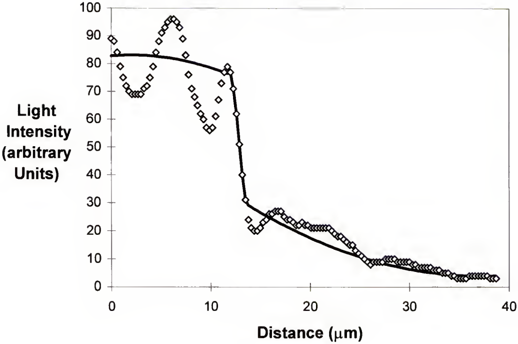

Figure 6-18 The measured edge response function of fused image plate with 2.8 μm diameter microfibers

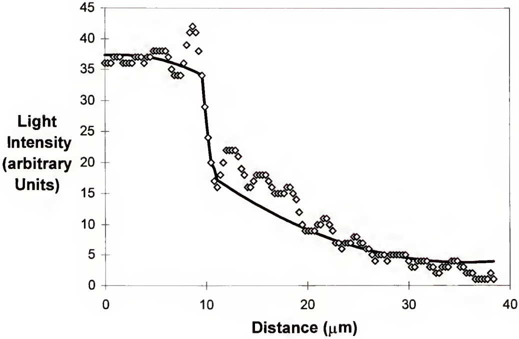

Figure 6-19 The measured edge response function of fused image plate with 2 μm diameter microfibers

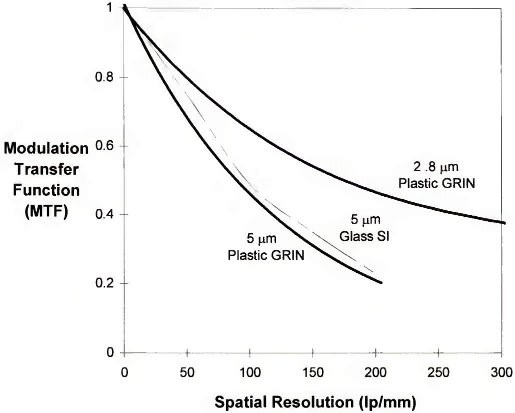

Figure 6-20 The modulation transfer functions of plastic GRIN image plates and glass SI image plate

6-4 Summary

In this chapter, the optical quality of the plastic GRIN image guides and fused image plates were characterized. In the case of image guides, the image brightness and the spatial resolution were evaluated and compared with those of glass SI image guides. The image brightness of the plastic GRIN image guide was more than a factor of two higher than that of the glass SI image guide with the same numerical aperture. Also image resolutions of the GRIN image guides were obtained by measuring the ERF of the transmitted image. The resultant MTFs were compared with those of published data from glass SI image guides. For the same 5 μm, microfiber diameter, plastic GRIN and glass SI image guides have similar spatial resolution. There is a significant improvement in resolution as the plastic microfiber diameter is reduced from 7 μm to 2.5 μm.

These results on the optical characterizations of plastic GRIN image guides have shown that it is possible to achieve ultrahigh resolution (less than 5μm) fiber-optic imaging. A factor of two improvement can be achieved in the resolution compared to state of the art glass SI image guide.

In addition, the image resolution of plastic GRIN fused image plates were measured. The MTF value of the GRIN image plate with 2.8 μm microfibers is about twice that with 5 μm microfibers. This result also shows that ultrahigh resolution (less than 5 μm) fused image plates can be made from plastic GRIN fibers with superior properties than plates made from glass SI fibers.

CHAPTER 7
CONCLUSIONS AND SUGGESTIONS FOR FUTURE WORK

7-1 Conclusions

Existing fiber-optic endoscopes and fused image plates are made from glass step index (SI) fibers. These fiber-optic devices made from SI fibers have a limitation in image resolution and image brightness because of their core/cladding structure. The optimum core/cladding ratio of SI fiber for highest resolution imaging equals 3.0 i.e., when the diameter of core is 3 μm and the cladding thickness is 1μm. Below 5 μm diameter microfiber, it has been found that if the core/cladding ratio is maintained at 3.0, and hence the cladding thickness is reduced, the image resolution is deteriorated due to the crosstalk and leaky rays phenomena. In addition, the image brightness is also reduced. Consequently, if the cladding thickness is maintained at 1 μm as fiber diameter is reduced below 5 μm, the brightness is rapidly reduced. Therefore, it may be concluded that ultrahigh resolution (less than 5 μm) fiber optic imaging can not be achieved using conventional SI type optical fibers.

On the theoretical side, it is expected that the crosstalk and leaky rays play a significant role in deteriorating image quality in ultrahigh resolution fiber-optic imaging. The coupling coefficient of SI fiber, which is related to the crosstalk between two SI profile fibers, is larger than that of Gaussian index profile fibers. And the effect of tunneling rays which are the main part of the leaky rays, in GRIN fiber are less than those of SI fiber, as was discussed in Chapter 3.

For this reason, the different type of optical fiber, i.e., plastic graded index (GRIN) fibers were used to fabricate an ultrahigh resolution image guide for ultrathin endoscopes and fused image plates. Plastic GRIN fibers were produced by drawing preformed polymeric rods. These rods were made by the interfacial-gel copolymerization technique. The MMA/BMA and MMA/VB monomer mixtures were polymerized to be used for GRIN image guides and fused image plates respectively because the MMA/BMA system has better transmittance, but lower numerical aperture than those of MMA/VB system.

To fabricate ultrahigh resolution image guides, a multiple drawing process was developed as described in Chapter 4. During the manufacturing processes, dust was the most critical parameter to deteriorate light transmission of the plastic GRIN image guide which has less than 5 μm diameter microfibers. To reduce the number of defects in the fiber or between fibers, a special cleaning and stacking method was developed.

Ultrahigh resolution plastic GRIN image guides with 7 μm, 5 μm, 3.5 μm and 2.5 μm diameter microfibers and fused image plates with 5 μm, 2.8 μm and 2 μm diameter microfibers were fabricated successfully. For GRIN image guides, the image brightness and the spatial resolution were measured to characterize the image quality and compared with those of glass SI image guides. For image plates, image resolutions were measured. The image brightness of the plastic GRIN image guide was more than a factor of two higher than that of the glass SI image guides with the same numerical aperture and same microfiber diameter. Also, image resolutions of the GRIN image guides were obtained by measuring the edge response function (ERF) of the transmitted sharp image. The resultant modulation transfer functions (MTF) were compared with those of known data from glass SI image guides. There is a significant improvement in spatial resolution of the plastic GRIN image guides as the microfiber diameter is reduced from 7 μm to 2.5 μm.

In addition, the image spatial resolution of plastic GRIN fused image plates were measured. The MTF value of the GRIN image plate with 2.8 μm microfibers is about twice that with 5 μm microfibers.

The most important conclusion of this feasibility study is that fiber-optic image guides made from polymeric graded index fibers can achieve ultrahigh image resolution, (i.e. below 5 μm) with better image brightness than that of SI image guides. The fundamental limitation on the resolution of all previous fiber-optic image guides imposed by the thickness of step index cladding materials can be overcome. This new technology applied to optical systems could have a major impact on a wide array of future optical systems used in defense, industrial and medical applications.

7-2 Suggestions for Future Work

7-2-1 Large Numerical Aperture GRIN Fiber

In this study, the feasibility was demonstrated for producing ultrahigh resolution plastic GRIN image guides and image plates containing microfibers whose diameters were in the range of 2.5 to 3.5 μm. Their optical resolution was measured to be about a factor of two higher than the existing glass SI fiber-optic image guides with 5 μm diameter microfibers. The GRIN fiber that was used to fabricate an ultrahigh resolution image guide had a numerical aperture of 0.23. If the numerical aperture of the GRIN fiber increases, the image quality of the image guide will be much better in image resolution and brightness. For light intensity limited applications, the larger numerical aperture will give a correspondingly greater light acceptance. That means, the image brightness can be much improved with higher numerical aperture fibers under the same lighting conditions. In addition, the image resolution also can be much improved, since the crosstalk which deteriorate image resolution, decreases as the numerical aperture of the fiber increases.

Therefore, it is very important to obtain a large numerical aperture GRIN fiber. As described in Chapter 2, blends of PMMA and the copolymer (75% Stylene + 25% Acrylonitrite) have been suggested. It has been known that the two polymers are completely miscible and the glass transition temperature is more than 100°C. The numerical aperture of this system will be 0.32.

Ultimately, fully fluorinated materials may be miscible and have a large difference in refractive index. These polymers need to be studied to obtain large numerical aperture plastic GRIN fibers.

7-2-2 Picosecond Tissue Imaging

GRIN fiber image guide can be applied to develop a tissue type sub-micron imaging through fluorescence lifetime measurement. It has recently been shown that tissue fluorescence lifetime differences in the range 10 picoseconds to 1 nanosecond can distinguish between specific types of tissue in the body. The fluorescence lifetime of various tissues have at least two exponential components with lifetime of a few hundred picoseconds and a few nanoseconds.

Every existing SI type fiber-optic image guide has an image time dispersion of about 100 times too great to permit their applicability for tissue identification. However, the GRIN image guide can permit essentially zero time dispersion (about 5 picoseconds) in the image transmission.

Therefore, it is possible to develop a novel fiber-optic endoscope using a plastic GRIN image guide that provides a bright image, an ultrahigh spatial resolution, and very short time dispersion for image acquisition. This very short time dispersion which is the unique characteristic of GRIN fiber, can open the new field of in-vivo biopsy in which cancerous tissue can be visualized.

REFERENCES

Adler, H., Fahrbach, G., and Stein, D. J. Crosslinking reactions in the rubber particles of high-impact polystyrene, Angew Chem., Int. Ed. Engl. 13(6) (1974).

Allan, W.B. Fibre optics theory and practice, Plenum Press, London (1973).

Andersson, P. S., Montan, S., Persson, T., Svanberg, S., Tapper, S., and Karlsson, S. E., Fluorescence endoscopy instrumentation for improved tissue characterization, Medi. Phys. 14, 632 (1987).

Ankiewicz, C., and Pask, C. Geometric optics approach to light acceptance and propagation in graded index fibers, Opt. Quant. Electr. 9, 87 (1977).

Ankiewicz, C., and Pask, C. Tunnelling rays in graded-index fibers, Opti. Quant. Electr. 10, 83 (1978).

Arnaud, J. A. Beam and fiber optics, Academic Press, New York (1976).

Artjushenko, V. G., Dianov, E. M., Konov, V. I., Mirakjan, M. M., Nikiforov, S. I., Prokhorov, M., Silenok, A. S., and Shcherbakov, I. A. Promising laser fiber systems for surgery, Opt. Fib. Medicine 4, SPIE 1067, 233 (1989).

Bown, S. G. Laser endoscopy, Briti. Medi. Bull. 42(3), 307 (1986).

Conde, R., Depeursinge, C., Coquoz, O. and Taleblou, F. Image quality in microendoscopy : Limiting factors, SPIE 2084, 87 (1994).

Costa, B., and Sordo, B. Optical fiber communication, McGraw-Hill, New York (1981).

Dowling, K., Dayel, M. K., Lever, M. J., French, P. M. W., Hares, J. D., and Dymoke-Bradshaw, L. Fluorescence lifetime imaging with picosecond resolution for biomedical application, Opt. Lett. 23, 810 (1998).

Duffieux, P. M. The Fourier transform and its applications to optics, 2nd ed. Wiley Interscience, New York (1983).

Eisel, U. Introduction to polymer physics, Wiley, New York (1990).

Gaskill, K. Linear systems, Fourier transforms and optics, Wiley, New York (1978).

Ghatak, A. K., and Thyagarajan, K. Contemporary optics, Plenum Press, London (1978).

Gloge, D., and Marcatili, E. A. J. Multimode theory of graded-core fibers, Bell System Technical Journal 52 (9), 1563 (1973).

Halley, P. Fibre optic systems, Wiley, New York (1987).

Hamamatsu, Fiber optic plate Technical Information, Sep. (1996).

Hasegawa, B. H. The physics of medical X-ray imaging, 2nd ed. Med. Phys. Publishing, Madison Wisconsin (1991).

Haubrich, S.W History of endoscopy, Gastroenterologic Endoscopy 2 (1989).

Hecht, J. Understanding fiber optics, Howard W. Sams, Indianapolis (1987).

Hirschowitz, B. I. A personal history of the fiberscope, Gastrology 764, 864 (1979).

Ho B.C., Chen, J. H., Chen, W.C., Chang, Y. H., Chen, J. J., and Tseng, T. W. Graded index polymer fibers prepared by extrusion, Polymer J. 27, 310 (1995).

Hosono, T. Transmission characteristics of image fiber, Electro. Comm. Japan, 66-C (11), 111 (1983).

Huang, L., and Osterberg, U. Measurement of crosstalk in order packed image fiber bundle, SPIE 2536, 480 (1995).

Ishigure, T., Nihei, E., and Koike, Y. Graded index polymer optical fiber for high speed data communication, Appl. Opt.33 (19), 4261 (1994).

Ishigure, T., Nihei, E., and Koike, Y. Optimization of the refractive index distribution of high bandwidth GI polymer optical fiber based on both modal and material dispersion, Polymer J. 28, 272 (1996).

Ishigure, T., Satoh, M., Takanashi, O., Nihei, E., Nyu, T., Yamazaki, S., and Koike, Y. Formation of the refractive index profile in the graded index polymer optical fiber gigabit data transmission, J. of Lightwave Technology 15, 2095 (1987).

Kapany, N. S. Fiber optics, Sci. Am. 203-5, 72 (1960).

Kapany, N. S. Fiber optics: Principles and applications, Academic Press, New York (1967).

Kapany, N. S., and Burke, J. J. Various image assessment parameters, J. Optical Soc. Am. 52, 1351 (1962).

Katzir, A. Optical fiber techniques, Encycloped. Phys. Sci. Tech. 9, 630 (1987).

Katzir, A. Optical fiber in medicine, Sci. Am. 260(5), 120 (1989).

Kawahara, I., and Ichikawa, H. Fiberoptic instrument technology, Gastro. Endosc. 20 (1987)

Kiat, L. S., Tanaka, K., Tsmanuma, T., and Sanada, K. Ultrathin single mode image fiber for medical usage, SPIE 1649, Opt. Fib. in Medicine 7, 208 (1992).

Koike, Y. High bandwidth graded index polymer optical fiber, Polymer 32, 1737 (1991).

Koike, Y., Hatanaka, H., and Ohtsuka, Y. Studies on the light-focusing plastic rod. 17: Plastic GRIN rod lens prepared by photocopolymerization of a ternary monomer system, Appl. Opt. 23, 1779 (1984).

Koike, Y., Hondo, Y., and Nihei, E. Graded-index optical fiber by new random copolymerization technique, SPIE 1592, 62 (1991).

Koike, Y., and Nihei, E. Method of manufacturing a graded optical transmission medium made of synthetic resin, U.S. Patent 5 253 323 (1993).

Koike, Y., and Nihei, E. Method of manufacturing optical transmission medium from synthetic resin, U.S. Patent 5 382 448 (1995).

Koike, Y., and Nihei, E. Method of manufacturing plastic optical transmission medium, U.S. Patent 5 593 621 (1997).

Koike, Y., Takezawa, Y., and Ohtsuka, Y. New interfacial-gel copolymerization technique for steric GRIN polymer optical waveguides and lens array, Appl. Opt. 27, 486 (1988).

Komiyama, A., and Hashimoto, M. Crosstalk and mode coupling between cores of image fibers, Electr. Lett. 25, 1105 (1989).

Komiyama, A., and Hashimoto M. A new class of crosstalk in image fibers, Opt. Comm. 107, 49 (1994).

Landry, M. R., Massa, D. J., Landry, C. J. T., Teegarden, D. M., Colby, R. H., and Long T.E. A survey of polyvinylphenol blend miscibility, J. Appl. Polym. Sci. 54, 991 (1994).

Leiner, D. C., and Prescott R. Correction of cromatic aberrations in GRIN endoscopes, Appl. Opt. 22(3), 383 (1983).

Lindstrom, L. H. Miniaturized pressure transducer intended for intravascular use, IEEE Transaction on Bio-Medi. Eng. 207 (1970).

Love, J. D., Pask, C., and Winkler, C. Rays and modes on step-index multimode elliptical waveguides, Micro waves, Opt. Acous. 3, 231 (1979).

Marcuse, D. Light transmission optics, Van Nostrand Reinhold, New York (1972).

McIntyre, P., and Snyder, A. W. Power transfer between optical fibers, J. Opt. Soc. Am. 65, 810 (1973).

Meyer-Arendt, J. R. Introduction to classical and modern Optics, 3rd ed. Prentice Hall, Englewood Cliffs, NJ (1989).

Nishi, H., Ichikawa, H., Toyama, M., and Kitano, I. Gradient-index objective lens for compact disk system, Appl. Opt. 25(19), 3340 (1986).

Ohtsuka, Y., Nihei, E., and Koike, Y. Graded index optical fibers of methyl methacrylate-vynyl benzoate copolymer with low loss and high bandwidth, Appl. Phys. Lett. 57(2), 120 (1990).

Olabisi, O. Polymer-polymer miscibility, Academic Press, New York (1979).

Park, C.-W., and Lee, B. A new method for the fabrication of cylindrical objects with radially varying properties, Indus. Eng. Chem. (to be published) (1999).

Paul, D. R., and Newman S. Polymer blends, Academic Press, New York (1978).

Paul, D. R., and Sperling, L.H. Multi-component polymer material, Am. Chem. Soc. (1986).

Pearson, A.D., French, W.G., and Rawson, E.G. Preparation of a light focusing glass rod by ion-exchange technique, Appl. Phys. Lett. 15(2), 76 (1969).

Pickering, M. A., Taylor, R. L., and Moor, D. T. Gradient infrared optical material prepared by a chemical vapor deposition process, Appl. Opt. 25(19), 3364 (1986).

Rees, J. D. Non-Gaussian imaging properties of GRIN fiber lens arrays, Appl. Opt. 21(6), 1009 (1982).

Rol, P., Jenny, R., Beck, D., Frankhauser, F., and Niederer, P. F. Optical properties of miniaturized endoscopes for ophthalmic use, Opt. Eng. 34(7), 2070 (1995).

Salmon, P. R. Fiber-optic endoscopy, Grune & Stratton, New York (1974).

Samuels, J. E., and Moore, D. T. Gradient-index profile control from mixed molten salt baths, Appl. Opt. 29(28), 4042 (1990).

Shingyouchi K., and Konishi S. Gradient-index doped silica rod lenses produced by a sol-gel method, Appl. Opt. 29, 4061 (1990).

Snyder, A. W., and Love, J. D. Tunneling leaky rays on optical waveguides, Opt. Comm. 12, 326 (1974).

Snyder, A. W., and Love, J. D. Optical waveguide theory, Chapman and Hall, New York (1983).

Snyder, A. W., and McIntyre, P. Crosstalk between light pipes, J. Opt. Soc. Am. 66, 877 (1976).

Snyder, A. W., and Mitchell, D. J. Leaky rays on circular optical fibers, J. Opt. Soc. Am. 64, 599 (1974).

Snyder, A. W., Mitchell, D. J., and Pask, C. Failure of geometric optics for analysis of circular optical fibers, J. Opt. Soc. Am. 64, 608 (1974).

Sperling, L. H. Introduction to physical polymer science, Wiley, New York (1992).

Struik, L.C.E. Internal stresses, dimensional instabilities, and molecular orientations in Plastics, Wiley, Chichester, England (1990).

Tanaka, T., and Benedek, G. B. Measurement of the velocity of blood flow (in vivo) using a fiber optic catheter and optical mixing spectroscopy, Appl. Opt. 14(1), 189 (1975).

Tsumanuma, T., Tanaka, K., Chigira, S., Sanada, K., and Inada, K. The ultrathin silica based imagefiber for the medical usage, Opt. Fib. Medicine 3, SPIE 906, 92 (1988).

Tsumanuma, T., Tanaka, T., Seto, K., Sanada, K., and Inada, K. New ultrathin needle scope used for diagnosis of small parts, SPIE 1067, 182 (1989).

Tsumanuma, T. Toriya, T., Tanaka, T., Samoto, N., Seto, K., and Sanada, K. New image diagnosis system with ultrathin endoscope and clinical results, SPIE 1420, 193 (1991).

Utrachi, L. A., Walsh, D. J., and Weiss R. A. Multiphase polymer: blends and ionomers, Acad. Chem. Soc. (1989).

Wang, Y., Brennan, A. B., Tymianski, J. R., and Walker, J. K. Plastic fiberoptic image guides for endoscopes, ANTEC 3367 (1995).

Woldarczyk, L. H. Dual wavelength catheter-type fiber optic pressure sensor, Opt. Fib. Medicine 4, SPIE 1067, 8 (1989).

Yamaguchi, S., Shimogima A., and Hosono T. Analysis of transmission characteristics of image fiber-Dependence on higher modes and wavelength, Electro. Comm. Japan, Part 2, 72(7), 51 (1989).

Yeh, C. Handbook of fiber optics theory and application, Academic Press, New York (1990).

BIOGRAPHICAL SKETCH

Bongsoo Lee was born on June 28, 1965, in Seoul, Korea. In 1984, he graduated with honors from WhiMoon High School in Seoul Korea. He received his Bachelor of Science and Master of Science in Nuclear Engineering from Seoul National University in 1989 and in 1991. He joined Korean Air force in 1991 as an official. In 1992, he married Seunghyun Cho and they had a son, Chungwon Lee in 1993. During his military service, he worked in the Ministry of Korean Defense from 1993 to 1995. He passed the Korean Government Overseas Scholarship examination in 1994, and he started his study toward Doctor of Philosophy at the University of Florida, Gainesville, in the fall of 1995. Currently, he is a candidate for the degree of Doctor of Philosophy in August 1999. He has been honored to receive the Nanoptics Inc. Fellowship since 1996.

I certify that I have read this study and that in my opinion it conforms to acceptable standards of scholarly presentation and is fully adequate, in scope and quality, as a dissertation for the degree of Doctor of Philosophy.

Wesley E. Bolch

Wesley E. Bolch, Chair
Associate Professor of Nuclear and
Radiological Engineering

I certify that I have read this study and that in my opinion it conforms to acceptable standards of scholarly presentation and is fully adequate, in scope and quality, as a dissertation for the degree of Doctor of Philosophy.

Alan M Jacobs

Alan M. Jacobs
Professor of Nuclear and Radiological
Engineering

I certify that I have read this study and that in my opinion it conforms to acceptable standards of scholarly presentation and is fully adequate, in scope and quality, as a dissertation for the degree of Doctor of Philosophy.

Samim Anghaie

Samim Anghaie
Professor of Nuclear and Radiological
Engineering

I certify that I have read this study and that in my opinion it conforms to acceptable standards of scholarly presentation and is fully adequate, in scope and quality, as a dissertation for the degree of Doctor of Philosophy.

James K. Walker

James K. Walker
Professor of Physics

I certify that I have read this study and that in my opinion it conforms to acceptable standards of scholarly presentation and is fully adequate, in scope and quality, as a dissertation for the degree of Doctor of Philosophy.

Won Young Choi
Vice-President Nanoptics, Inc.

This dissertation was submitted to the Graduate Faculty of the College of Engineering and to the Graduate School and was accepted as partial fulfillment of the requirements for the degree of Doctor of Philosophy

August 1999

Dean, College of Engineering

Dean, Graduate School